university of groningen

faculty of science and engineering

BSc Thesis

Cosmic Voids: Persistence and Hierarchy within the density and potential field

Thomas Bruinse

university of groningen / faculty of science and engineering

University of Groningen

Cosmic Voids: Persistence and Hierarchy within the potential and density field

Bachelor's Thesis

To fulfill the requirements for the degree of
Bachelor of Science in Astronomy
at University of Groningen

Under the supervision of

Prof. dr. Rien van de Weygaert (Kapteyn Astronomical Institute, University of Groningen)
and
Georg Wilding (Kapteyn Astronomical Institute, University of Groningen)

July 15, 2021

Contents

Page

Acknowledgments **4**

Abstract **5**

1 Introduction **6**

2 The Cosmic Web **7**
2.1 The Megaparsec Universe 7
2.2 Formation of Structure 8
2.3 Voids 10
2.3.1 Formation and Evolution of Voids 10
2.3.2 Void Dynamics 12
2.3.3 Void Hierarchy 15

3 Topological Data Analysis **17**
3.1 Delaunay and Alpha Complex 17
3.2 Watershed Transform 19
3.3 Morse-Smale Complex and Persistence 20
3.4 Application to the Cosmic Web 23

4 Results I: Void Hierarchy **25**
4.1 Density Field Filtration 25
4.2 Watershed Transform versus Morse-Smale Complex 26
4.3 Watershed Comparison 26
4.4 Void Shapes 27

5 Results II: The Topology of the Potential Field **33**
5.1 Gravitational Potential 33
5.2 Persistence 34

6 Conclusion **37**
6.1 On WVF and the Potential 37
6.2 Issues with the Void Shapes 38
6.3 Further Research 39
6.3.1 Ellipsoid Fits 39
6.3.2 Substructure Remnants 39
6.3.3 Velocity Field 39
6.3.4 Sachs-Wolfe Effect 39

Bibliography **42**

Acknowledgments

I wish to thank Rien and Georg for their patience while guiding me through this project. I'm glad I chose you to work with.

Abstract

As cosmic voids are a very prominent component of the cosmic web, a great deal of attention goes towards discovering their structure and their effect on the other cosmic constituents. Because the gravitational force field is very weak inside these big near-empty regions with sizes of roughly 20 to 50 h^{-1} Mpc, they form unique laboratories to probe the effect of dark energy by looking at their their shape and evolution. Topological Data Analysis (TDA) and watershed transforms provide a great method to reveal their sizes and shapes, together with their rich hierarchical structure. Watershed Void Finder (WVF) can be used as a tool for the identification and segmentation of voids, by choosing the right threshold parameters. The topology of voids will be described by looking at their persistence, based on the concept of the Morse-Smale complex. Voids will then be found through the critical points in the density field. Their shapes can be approximated by fitting an ellipsoid. By transforming the density field to a gravitational field through Poisson's equation, the same analysis can be done on the potential. Their features can be compared to give more insight into the dynamics of voids. A more thorough study of the gravitational potential field at various redshifts might then provide a better understanding of the Sachs-Wolfe effect and its connection to the temperature fluctuations in the Cosmic Microwave Background (CMB).

1 Introduction

Voids are an important part of the large-scale structure of the universe and have a great impact on the dynamics and evolution of their surroundings. These near-empty regions hold valuable remnants of the early universe, as their structure and formation strongly depend on the anisotropies in the primordial density field. As such, voids hold precious information on the past, present and future of the universe. Deep within these voids we find pristine underdense regions where we can probe the nature of gravity and dark energy.

To be able to reveal its hidden secrets, we need a strong mathematical foundation to understand the geometry of the cosmic web through simulations. This foundation can be found in topology, which describes the properties of geometric objects that are preserved under continuous deformations. The components of the cosmic web experience deformations constantly, caused by the tidal force field and gravitational instabilities, making topology a suitable method to study their geometric features. Identifying these properties which are preserved throughout the evolution of structure formation in the cosmic web holds therefore a direct link to the very beginning stages of the universe. Studying the shape and structure of voids, as well as their influence on their surrounding, are of great importance.

In this thesis we will focus on the properties of voids using two methods which are closely related. First, we start off by giving some background information on the cosmic web, its components and their evolution. Then we will summarize the mathematical concepts on which our analysis will be based - the watershed transform and persistent topology.

Next we proceed by applying a watershed transform on a DTFE density field simulation. This will effectively identify and segregate the various voids within the density field. We will show how the shape and size of voids depend on the chosen parameters in the algorithm used to apply the watershed transform - Watershed Void Finder (WFV). Next, we derive the Morse-Smale complex from the critical points (maxima, minima and saddle points) of the density field. Voids can be identified by determining the threshold densities at which they emerge and and disappear - their persistence. The comparison between the watershed analysis and persistent topology will be the main focus.

The obtained voids found by these two methods can then be compared to check if there are any differences in their shape and size. These properties will be found by fitting ellipsoids through the voids. The fitting is done by choosing an ellipsoid which matches the inertia tensor of the void.

By converting the DTFE density field to its corresponding gravitational potential field through its Fourier decomposition, we are able to compare the persistence of topological features in both fields. Finally we will apply a watershed transform on the potential field. The difficulties that arise from this analysis and possible ideas for further research are discussed in the last chapter.

2 The Cosmic Web

2.1 The Megaparsec Universe

The invention of the ground-based telescope by Dutch spectacle-maker Hans Lippershey in 1608 allowed us to discover our solar system and its configuration. From here the telescope has gone through many developments and eventually evolved into a powerful tool to study the universe. By sending them to space in an orbit around the Earth, it has expanded the horizons of our observable universe by studying galaxies and galaxy clusters. Today, we are able to map the density of galaxies to redshifts beyond $z = 6$. The Sloan Digital Sky Survey (SDSS) made photometric observations of roughly one billion objects, covering 35 percent of the sky (see Figure 1). This immense study led us to identify sheets, filaments and clusters of galaxies with large near-empty regions in between, revealing the existence of the Cosmic Web (Blanton & SDSS 2014).

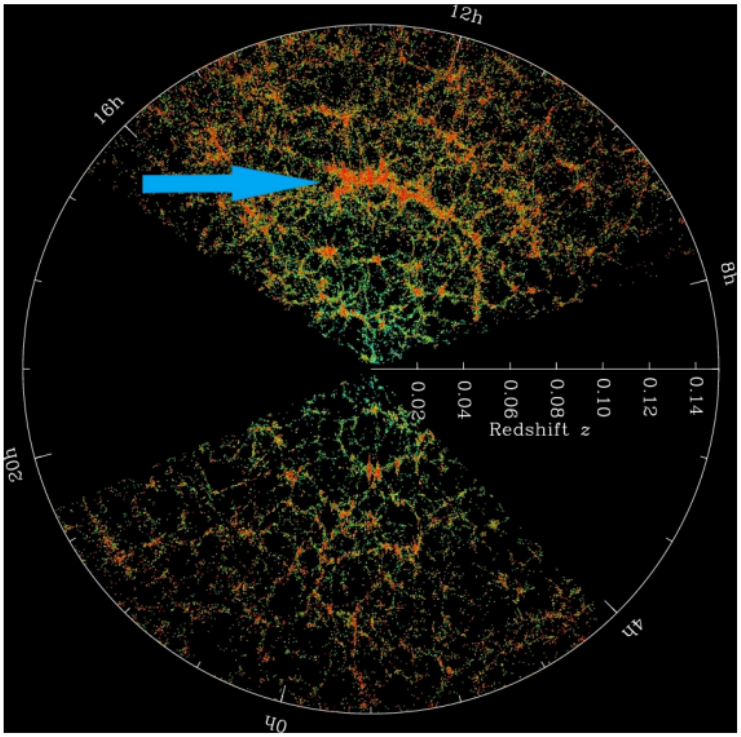

Figure 1: A map of the universe. Filaments, clusters and voids can be seen. The blue arrow points at the Sloan Great Wall (Blanton & SDSS 2014).

Considering these colossal distances in the Megaparsec universe and beyond, the universe is both homogeneous and isotropic - it looks the same in every direction no matter where we set up our telescope. This is known as the Cosmological Principle and these conditions only hold on 'large scales' of roughly 100 Mpc or more (van de Weygaert & Platen 2009). On smaller scales it becomes increasingly more anisotropic. Therefore the structure of the universe is profoundly dependent on the scale in which we choose to observe. The isotropic and homogeneous nature of the cosmos on large scales is directly visible in sophisticated simulations of the Cosmic Web (see Figure 2). As one of the most iconic and intriguing patterns found in nature, the Cosmic Web shows us the large-scale structure of the universe and the hierarchy of its components (van de Weygaert & Sheth 2003). Filaments and sheetlike walls are connected to clusters which confine voids of various sizes and shapes within.

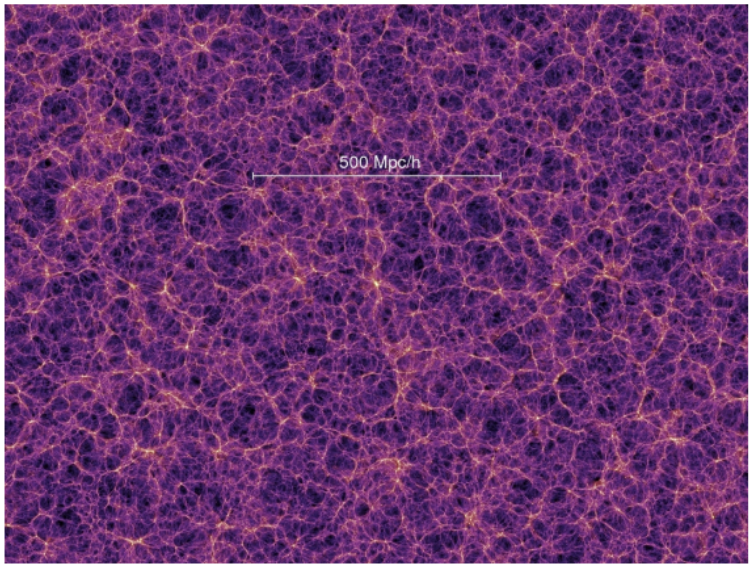

Figure 2: A two-dimensional slice through the Millennium simulation at redshift zero. The creation of the full simulation involved 10 billion dark matter particles in a three-dimensional space with more than 2 billion light-years width (Springel & Max-Planck-Institute 2005).

Density fluctuations in the galaxy distribution throughout the universe give rise to gravitational instabilities, which are (together with the large-scale tidal field) the main source for the creation of this web-like structure (Cautun et al. 2014). The density fluctuation at a specific point in space is defined as:

$$\delta(\vec{x},t) = \frac{\rho(\vec{x},t) - \rho_u(t)}{\rho_u(t)}$$

$\rho(\vec{x},t)$ is the absolute density, while ρ_u is the mean density in the universe. We can convert this to:

$$1 + \delta(\vec{x},t) = \frac{\rho(\vec{x},t)}{\rho_u(t)}$$

Its shows there is no limit to the overdensity ($\delta > 0$) - it can be arbitrarily large. There is a limit to the underdensity however, because δ cannot become smaller than -1. This leads to an asymmetry between the dense structures (walls, filaments, clusters) and the underdense structures (voids) (Cautun et al. 2014). The density PDF of each component is given in Figure 3.

2.2 Formation of Structure

The Zel'dovich formalism (Zel'Dovich 1970) is one of the key descriptions of the formation of structure in the universe. It states that the morphology of a structure depends on the eigenvalues of the deformation tensor. Eigenvalues of this tensor are related to the different components in the Cosmic Web. Voids correspond to regions with all negative eigenvalues. Sheets, filaments and clusters correspond to domains with one, two and three positive eigenvalues respectively. The Zel'dovich approximation then outlines the sequence in which anisotropic collapse occurs. Regions first contract to form walls, then they contract to form filaments and only at the end they fully collapse along each

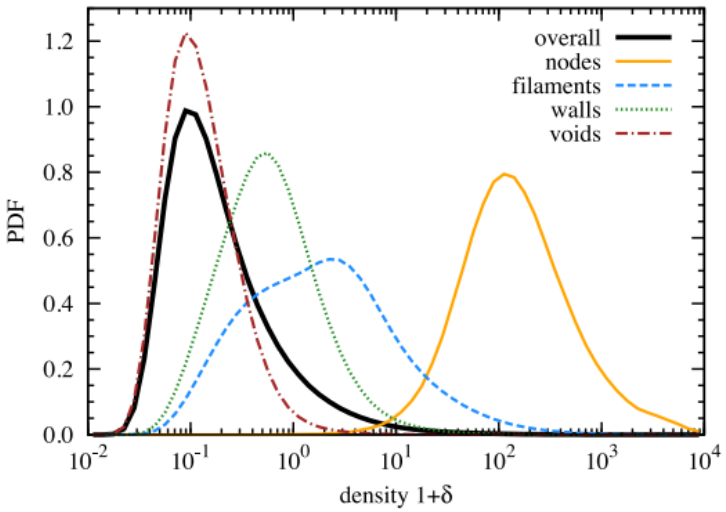

Figure 3: The PDF of the density in each component of the cosmic web. The results are obtained by using the NEXUS+ simulation (Cautun et al. 2014).

direction (Cautun et al. 2014). This description is also used to elucidate anisotropic gravitational collapse.

From the Lagrangian description of fluid motion (where the coordinate system moves along with the fluid element) we can convert the densities to the Eulerian view (where the coordinate system is fixed) through the following relation:

$$\rho(\vec{x},t)dx = \rho_u(t)dq$$

We can perform a perturbation to the density to check how the evolution of structure enfolds, depending on the deformation tensor:

$$1+\delta(\vec{x},t) = |\frac{\partial x}{\partial q}|^{-1} = |\delta_{mn} - D(t)\psi_{mn}|^{-1}$$

Here, $|\frac{\partial x}{\partial q}|^{-1}$ represents the determinant of the Jacobi matrix, $D(t)$ is the growth factor, δ_{mn} is the Kronecker delta, $\delta(\vec{x},t)$ is the density perturbation and ψ_{mn} is the deformation tensor. In this manner, the evolution of the perturbation is completely described by its eigenvalues $\lambda_1 \leq \lambda_2 \leq \lambda_3$ as follows:

$$1+\delta(\vec{x},t) = \frac{1}{|1-D(t)\lambda_1||1-D(t)\lambda_2||1-D(t)\lambda_3|}$$

The deformation tensor ψ_{mn} is related to the tidal tensor τ_{mn}:

$$\psi_{mn} = \frac{1}{\frac{3}{2}\Omega H^2 a(t)}\left(\underline{\tau}_{mn} + \frac{1}{2}\Omega H^2 \underline{\delta}(\vec{x},t)\delta_{mn}\right)$$

Ω is the density parameter, $a(t)$ is the scale factor, H is the Hubble constant, while $\underline{\tau}_{mn}$ and $\underline{\delta}(\vec{x},t)$ correspond to the linearly extrapolated values of the tidal shear tensor and the density perturbation.

The anisotropic collapse of matter by tidal forces goes in the direction of the positive eigenvalues, where a higher value results in a faster collapse. First it forms a wall (collapse in one direction), then

it forms a filament (collapse in two directions) and in the end the collapse occurs along each directions to form a cluster. Voids on the other hand, where matter flows towards the overdense structures, correspond to regions with all negative eigenvalues (Cautun et al. 2014).

By studying the eigenvalues of the deformation tensor in the primordial density field, Doroshkevich (1970) found that the morphological components emerging from this field are directly linked to the Zel'dovich formalism. This approach is able to describe the early linear phase of the evolution of the cosmic web, but slowly loses its viability as it enters the non-linear regime of structure formation (van de Weygaert & Sheth 2003). From the primordial density field, the overdense regions most likely evolve into filaments and clusters, while underdense regions are the seeds from where the growth of voids begin as the evolution of the cosmos continues.

2.3 Voids

Voids form a considerable share of the overall structure of the cosmic web . They form huge volumes of underdense regions ($\delta < 0$), roughly with sizes in the range of 20 to 50 h^{-1} Mpc. They are known to have a roundish shape, but are never perfectly spherical (van de Weygaert et al. 2012). To put it in perspective: the total mass share of cosmic voids is about 15 percent, while the total volume fraction is 77 percent of the cosmic web (see Figure 4), according to computer simulations of the LCDM universe e.g. the Millennium simulation. This implies the average density in voids is approximately 20 percent of the average cosmic density which matches the results of theoretical models (van de Weygaert 2016). Voids never exist on their own - they are encompassed by filaments, clusters and sheetlike walls. These boundaries determine its shape and its evolution. Their structure, morphology and dynamics form pristine laboratories to study the fundamental constants of nature in the Megaparsec universe. They are able to illuminate the obscurities of dark energy, dark matter and tell us something about possible non-Gaussianities in the primordial perturbation field (van de Weygaert 2016).

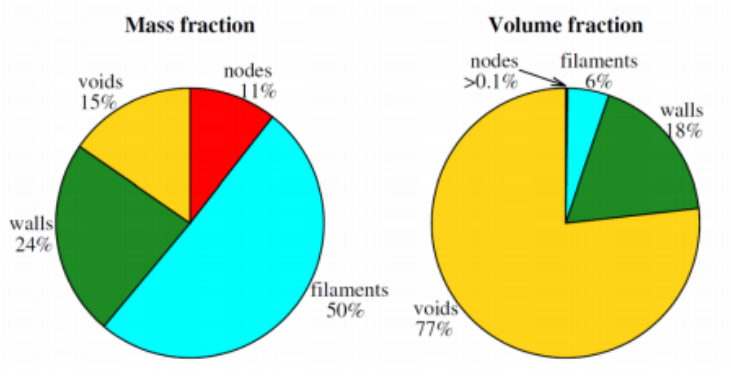

Figure 4: Mass fraction and volume fraction of the different components of the Cosmic Web (Cautun et al. 2014).

2.3.1 Formation and Evolution of Voids

The emergence of cosmic voids begins at the density troughs in the fluctuating primordial Gaussian density field. These fluctuations can be seen in the Cosmic Microwave Background (CMB) as mani-

festation of Heisenberg's uncertainty principle (see Figure 6) . While the universe expands, filaments, clusters and sheetlike walls are formed due to gravity. Initially overdense regions become more dense, while the underdense regions lose their density by out-flowing streams of matter towards filaments and clusters. As matter is gravitationally accelerated outwards, the expansion detaches from the Hubble flow and the voids appear to be expanding with respect to the background universe. Theoretically speaking, the ever decreasing density continues asymptotically until it reaches pure emptiness (van de Weygaert 2016). The eventual shape, alignment and dynamics of voids depend strongly on external tidal forces. They can merge with other voids and can collapse due to their surroundings.

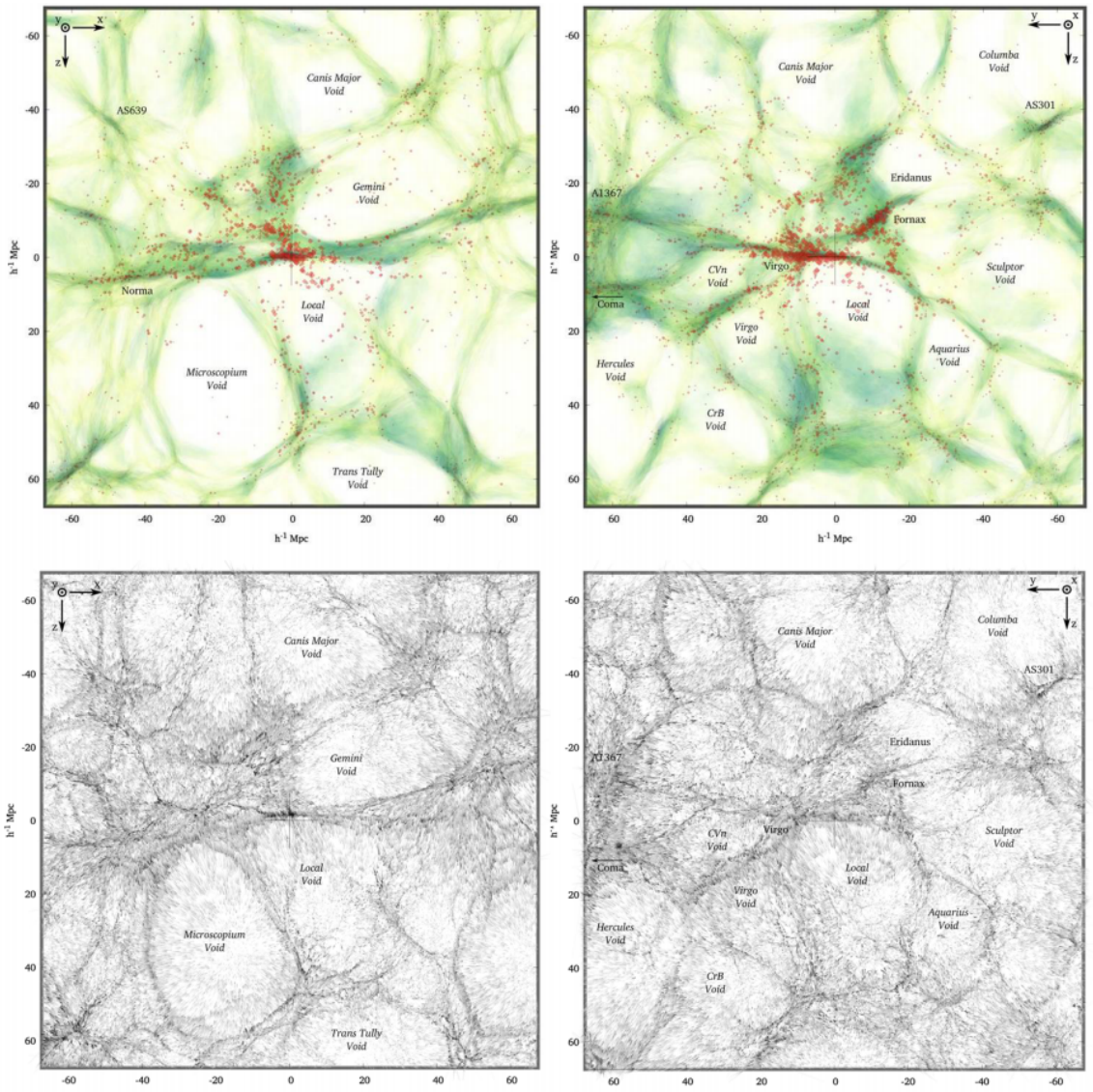

Figure 5: A map showing the voids in the Local Universe. It compares two perpendicular slices perpendicular to the plane of the Local Supercluster. Our location is pointed out by the cross. The top frame show how the weblike structure of the density field is reconstructed by using samples of the 2MRS survey (red dots). The bottom frames show the corresponding velocity flow where the ridges on the boundaries of voids can be seen clearly (Hidding et al. 2016).

Another possible effect on the shape of voids is the repulsive influence of dark energy on the force field, making voids an attractive spot to probe dark energy. An intricate study by Bos et al. (2012)

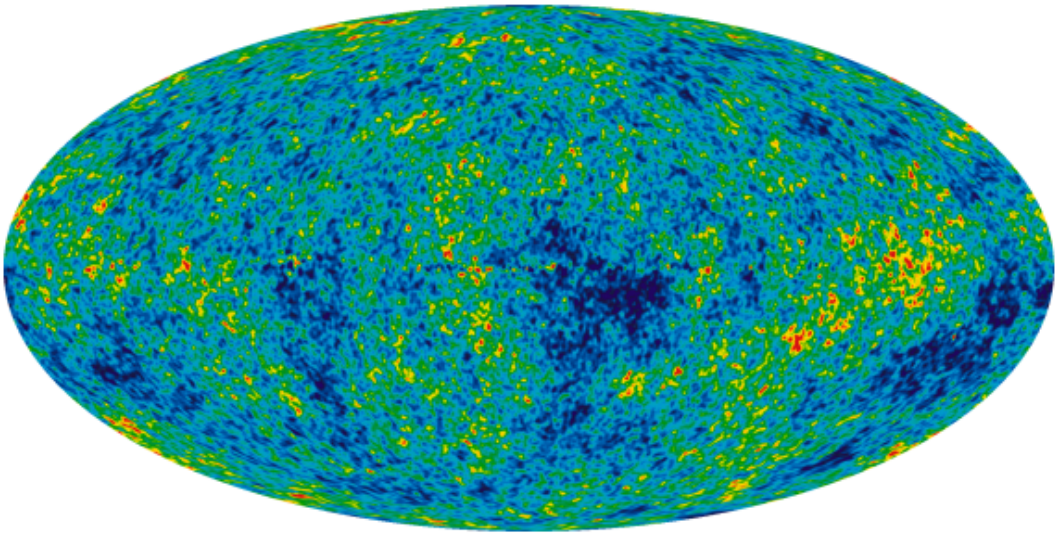

Figure 6: The Cosmic Microwave Background (CMB) from the WMAP data, showing the temperature fluctuations (Bennett et al. 2013).

showed Dark matter halos residing within voids are highly sensitive to dark energy, eventually determining the shape of the dark matter voids (van de Weygaert et al. 2012).

Computer simulations show that the evolution of voids due to gravity reveal a rich variation of structure, sizes and shapes. They outline void distributions consisting of many small-sized voids which are able to coexist inside one large void at an early epoch and merging all together at a later epoch. This confirms the hierarchical buildup of voids in the cosmic web (Dries 2008).

2.3.2 Void Dynamics

Various studies have found indications of voids influencing the peculiar velocity flows of galaxies in the Local Universe (Bothun & McGaugh 1992). In recent years, the dynamical effect within the Local Universe is understood in greater detail due to improved data samples (e.g. the 2MASS survey), providing a detailed analysis on the velocity field in our local cosmos. A study by Tully et al. (2008) shows the Local Void is having a repulsive influence on the Local Group accounting for approximately 259 km s^{-1} of the total 631 km s^{-1} with respect to the CMB. Two idealized configurations especially provide an insightful way of displaying the dynamics of voids - the spherically isolated void and the homogeneous ellipsoidal void. The spherical model describes the flow of matter within voids, while the ellipsoidal model allows us to understand the importance of the external tidal forces on the void dynamics (van de Weygaert & Platen 2009).

While it is proven that voids will never be able to become perfectly spherical, the spherical void model is still able to give a description of the expansion of voids in a simple and clarifying fashion. It shows how a ridge around the expanding void is formed as a result of the differential outward expansion of the mass around the void and within. Near the boundary, the inner mass layers move outwards faster than the outward layers. This happens because the outer layers feel a more moderate interior underdesnity. This eventually leads to the inner shell taking over the outer shell, which defines the

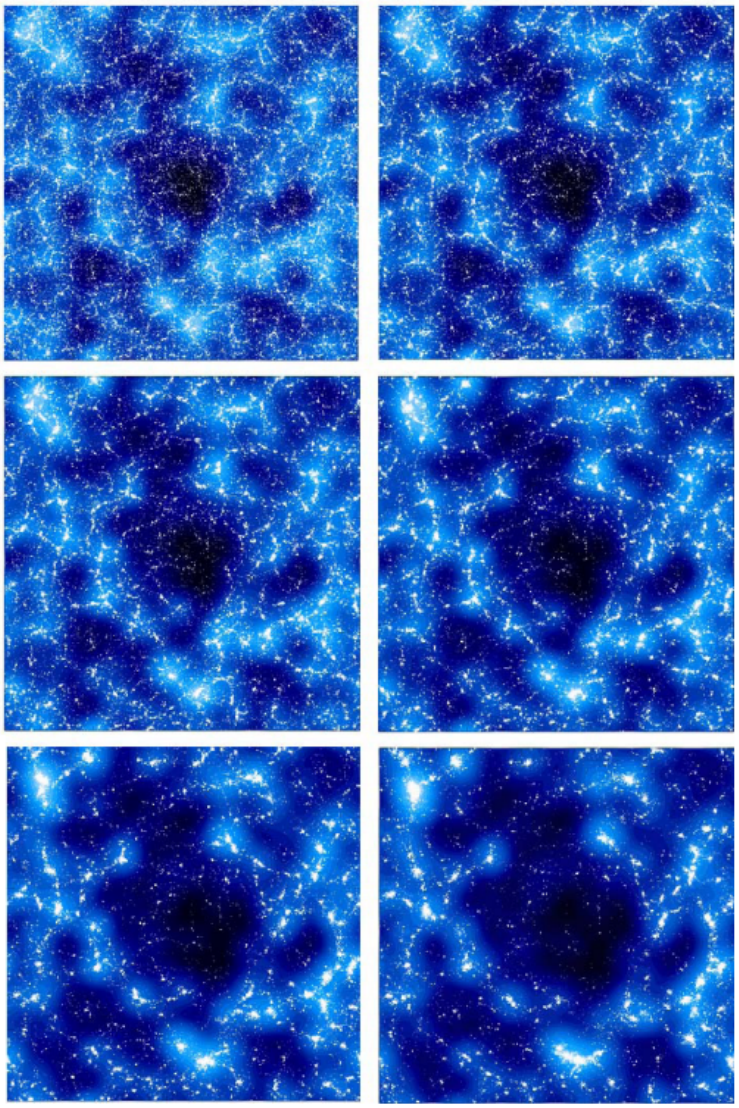

Figure 7: Simulation of an evolving void in a LCDM Universe. The slice is 50 h^{-1} Mpc by 10 h^{-1} Mpc. The images show particles within a density field, which is smoothed on a scale of 4 h^{-1} Mpc. The evolution of the void is given in timesteps (a= 0.05, 0.15, 0.35, 0.55, 0.75 and 1.0) (Platen 2009).

evolutionary timescale for void evolution - the shellcrossing timescale (van de Weygaert & Platen 2009). This leads to the accumulation of mass near the boundary, while evening out the density distribution in the interior. Once voids pass the stage of shellcrossing, their expansion slows down. This allows us to identify voids which are in the present-day galaxy distribution from the voids that just reached the stage of shellcrossing (van de Weygaert & Platen 2009). From Figure 8 we can see voids will evolve into a bucket shaped profile despite using different initial conditions with uniform density in the interior and a jump in the density near the boundary, showing the bucked shaped density profile is a generic property of cosmic voids. However, this is a theoretical model. In practice voids never become perfectly spherical and therefore their density profiles have a less prominent bucket shaped interior profile compared to those in the left panel of Figure 8. Spherical averaging will eventually lead to the mixing of different layers in the void's interior, preventing a perfect bucket shaped interior.

Even though the spherical void model describes the evolution of the density distribution from within,

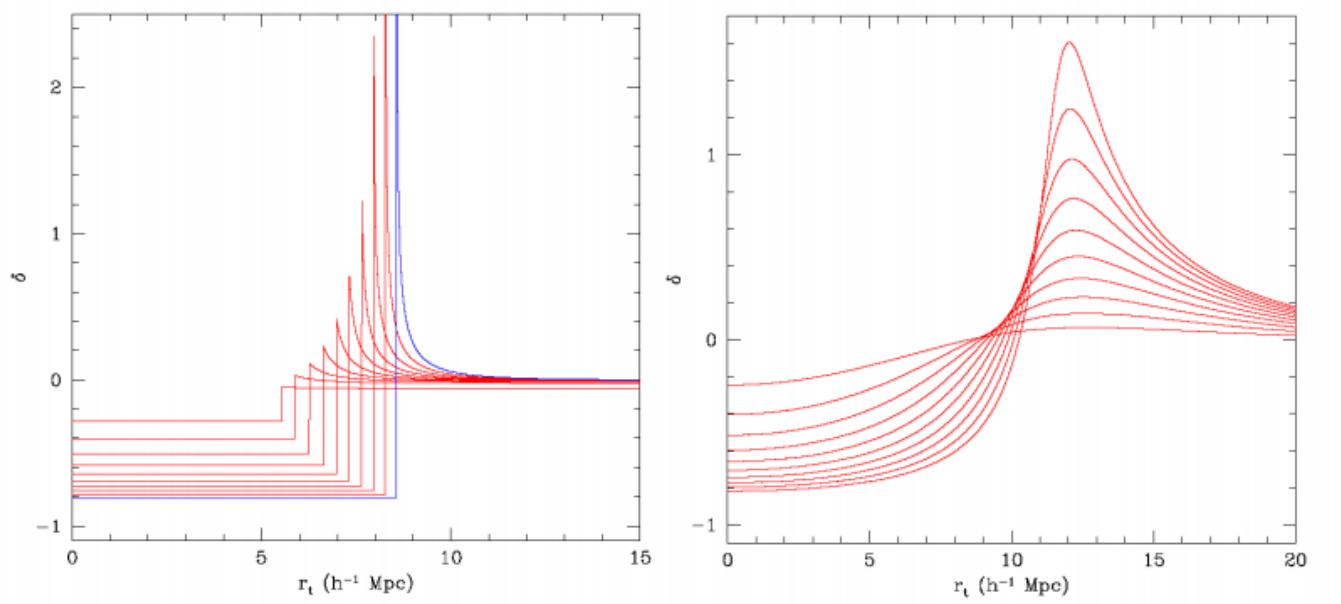

Figure 8: Spherical models for the evolution of voids with a wide range of initial radial profiles. Left panel shows a pure void evolving to the epoch of shellcrossing. Righ panel shows a void with an angular averaged density profile from a Gaussian random field (SCDM profile). Because of the differential expansion of the mass shells inside the void, there is an accumulation of mass near its boundary. This accumulation of mass can be seen from the the peak that is formed (van de Weygaert 2016).

it fails to describe the effect of the exterior on the void's boundaries. The ellipsoidal model by Icke (1984) probes the role of external tidal forces on the evolution of voids by considering homogeneous underdense ellipsoids (van de Weygaert & Platen 2009). This approximation is restricted to the fairly homogeneous interior, and fails at the void's boundaries were density fluctuations are more prominent. The model describes how the large-scale near-linear tidal field will decline as the density fluctuation δ grows strongly non-linear. This is understood from the gravitational acceleration along the ellipsoid's principle axes, which can be evaluated from the scale factors R_i:

$$\frac{d^2R_m}{dt^2} = -4\pi\rho_u G\left[\frac{1+\delta}{3} + \frac{1}{2}(\alpha_m - \frac{2}{3})\delta\right]R_m - \tau_m R_m + \Lambda R_m$$

Where Λ is the cosmological constant, τ_m is the eigenvalue of the tidal shear tensor and ρ_u is the uniform background density embedding the interior density of the homogeneous ellipsoid. The ellipsoidal coefficients $\alpha_m(t)$ are found by the integral equation:

$$\alpha_m(t) = R_1(t)R_2(t)R_3(t)\int_0^\infty \frac{d\lambda}{(R_m^2(t)+\lambda)\prod_n^3(R_n^2(t)+\lambda)^{1/2}}$$

Because the density deficit δ can never be smaller than -1, the importance of the tidal shear effect through τ_m remains relatively high. The tidal forces from the exterior cause voids to expand anisotropically and can even trigger their collapse. The tidal shear tensor is the main reason preventing voids of obtaining a perfectly spherical shape. Voids also tend to align with the tidal force field generated by large-scale structures of at least 20 to 30 h^{-1} Mpc, contributing considerably to the formation of structure in the Megaparsec universe (van de Weygaert & Platen 2009).

2.3.3 Void Hierarchy

The evolutionary path of voids is dominated by two processes: merging and collapse (Dries 2008). The eventual fate of small voids depends on their exterior. If they are embedded in a larger void - they gradually merge (void-in-void configuration). If they are surrounded by overdense regions - they are squeezed and prone to collapse (void-in-cloud configuration). The hierarchical formation and development of voids can be explained by the two-barrier excursion set formalism (Sheth & van de Weygaert 2003). We can define the linearly extrapolated primordial density fluctuation on a scale R:

$$\delta_L(\vec{x},t)|R) = \frac{D(t)}{D(t_i)})\delta_L(\vec{x},t_i|R)$$

Where $D(t)$ is the linear density growth factor. If $\delta_L(\vec{x},t)|R)$ exceeds the the density threshold (depending on which cosmological model we use), it will collapse. A void will be formed when an underdensity reaches the critical density threshold of the shell-crossing phase. As voids emerge from the primordial Gaussian random field, small ones coexist within large ones. At a later epoch they will eventually merge. Voids embedded in collapsing regions will be squeezed and disappear. To determine the total void count, we would have to take into account these two processes. The two-barrier formalism for voids shows their hierarchical buildup is much more complex than for overdense regioins. For the latter, the two-barrier formalism becomes more straightforward because a filament or cluster isn't torn apart as the surrounding void expands (van de Weygaert & Sheth 2003).

The creation and destruction of voids has an important effect on its observed hierarchy. To study this hierarchy in more detail we need a mathematical framework which allows us to identify the geometric properties of the cosmic web.

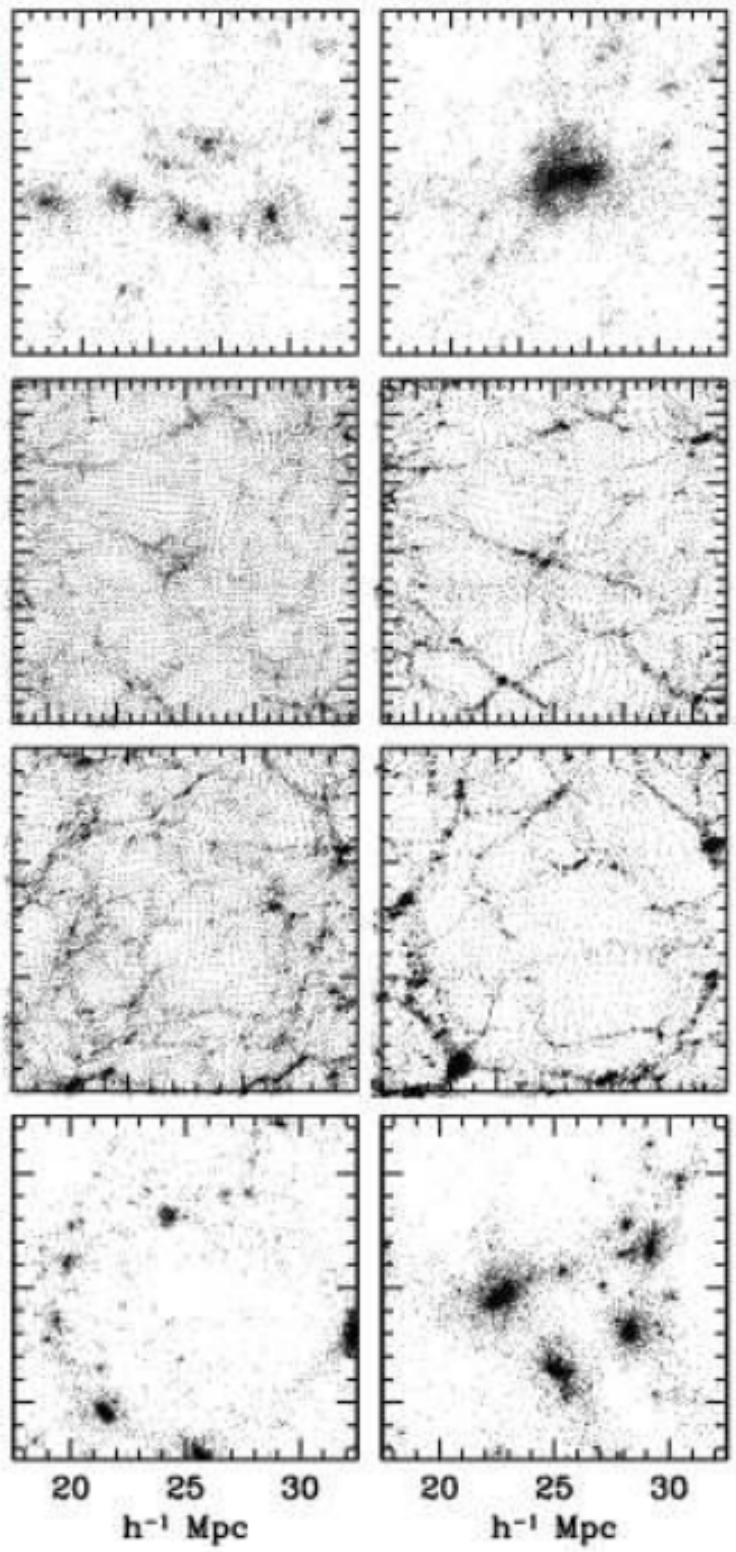

Figure 9: These images illustrate a configuration of overdense clouds and underdense voids, comparing an earlier epoch (left) with a later epoch (right). From top to bottom it shows a cloud-in-cloud, cloud-in-void, void-in-void and void-in-cloud configuration. Comparing the cloud-in-void and void-in-cloud configurations (second row and last row respectively), we see that high-density halos are still visible within expanding voids while voids within collapsed halos are not (van de Weygaert & Sheth 2003).

3 Topological Data Analysis

Recent developments in high performance computing has led to an immense volume of scientific data from astronomical simulations. As the amount of data-sets from these simulations keep rising, the importance of efficient ways to process and interpret it becomes greater as well. Suitable methods would have to find a balance between maximizing the amount of information gained and minimizing the computational power needed.

Topological Data Analysis (TDA) is such a method to analyse great volumes of data and can be applied to many scientific fields. Recent years TDA gained popularity among cosmologists to reduce and analyse arguably the most extreme case of Big Data - large scale structure simulations of the cosmos (van de Weygaert et al. 2013). It is a broad set of tools based on mathematical concepts in the field of topology dealing with structures, its components and its features through different dimensions. One of the subfields of TDA with a high applicability in describing and analysing the cosmic web is persistent homology (Pranav et al. 2017). It concerns multidimensional representations of loops and categorizes them in homology groups. To study the cosmic web in more detail we can look at the persistence of these homology groups throughout its hierarchical structure.

A topological description of the universe is a powerful and insightful way to expose its geometry and morphological features. While it is not possible to fully characterize the topology of the universe by simulations due to lack of computational speed, it is feasible to outline the ranks of homology groups which describe the multiscale structure of the universe (Wilding 2018). The availability of fast algorithms to compute the homology ranks accompanied with their rich information, makes it an attractive way to study the formation of structure in the universe.

The rank (the number of independent elements) of these groups are known as Betti numbers and they are a characterization of the topology of orientable 2-manifolds, which can be used to summarize the topology of the cosmic web. The three Betti numbers β_0, β_1, β_2, define the dimension of holes in the cosmic mass distribution. These holes are related to features we find in the cosmic web. Each Betti number represents the dimension needed to enclose the holes. Applying this to the description to the cosmic web: β_0 describes the connectedness through clusters, β_1 corresponds to tunnels through the cosmic structure, β_2 corresponds to cosmic voids. By counting the number of β_0, β_1 and β_2 we also count the number of these features that are present in a sample volume of the cosmic web (Wilding et al. 2021). Not only are Betti numbers used to count components of the cosmic structure, but also provide valuable insight to their separation, combination and merging (Wilding 2018). This can be used to describe the evolution of structure in the universe and compare different cosmologies other than the LCDM model and provide insight if a possible modification of our theory of gravity is needed.

3.1 Delaunay and Alpha Complex

Important aspects to the decomposition of the cosmic web in such a way we can describe it with a mathematical framework based on topological features are the Alpha and Delaunay complexes (Edelsbrunner & Mücke 1994). The construction of the Delaunay complex consists of a few steps. First we construct the Voronoi regions of a point set (seeds). This is defined to be the region around a seed in the set, consisting of all points of the plane closer to that seed than to any other (see Figure 10). Delaunay triangulations can be made by connecting all the seeds if and only if their Voronoi regions

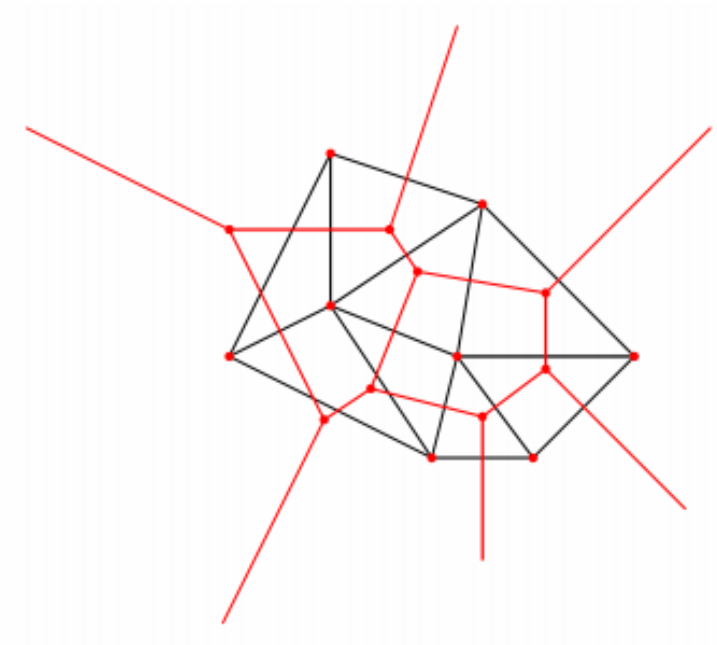

Figure 10: Voronoi regions of a set of points (red) with their corresponding Delaunay triangulation (black) (Vegter 2011).

share a common line segment (the black lines in Figure 10). The edges of the faces then form the simplices of the triangulation: the Delaunay complex.

We can extend this process by taking the union of closed balls with radius α, centred around the seeds in our set. In this case the regions are all the points closer to a specific seed than any other seed within the ball. Intersecting these regions with the Voronoi regions creates simplices which form the Alpha complex (Edelsbrunner & Mücke 1994). The union of all the simplices in the Alpha complex is then the Alpha shape.

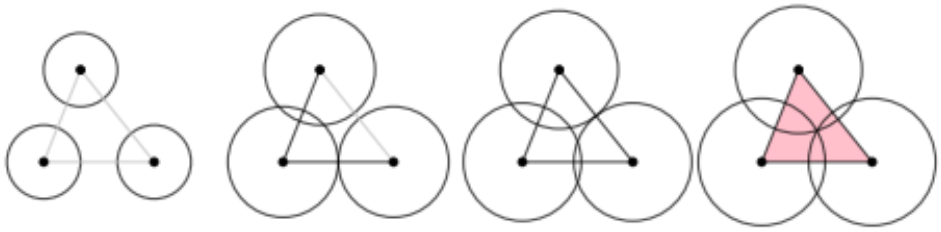

Figure 11: Constructing the Alpha Complex. The vertices only connect when the radii of the balls overlap (Wilding 2018).

This procedure can be extended to three dimensions. As the radius α increases, new simplices will be added to the complex (see Figure 11 and Figure 12) until a value of α is reached which returns the Delaunay complex. The thresholds chosen for radius α directly determine the Alpha complex and the Alpha shape (Edelsbrunner & Mücke 1994). This concept of thresholding plays a key part in unveiling the hierarchy of the components in the cosmic web (van de Weygaert & Sheth 2003).

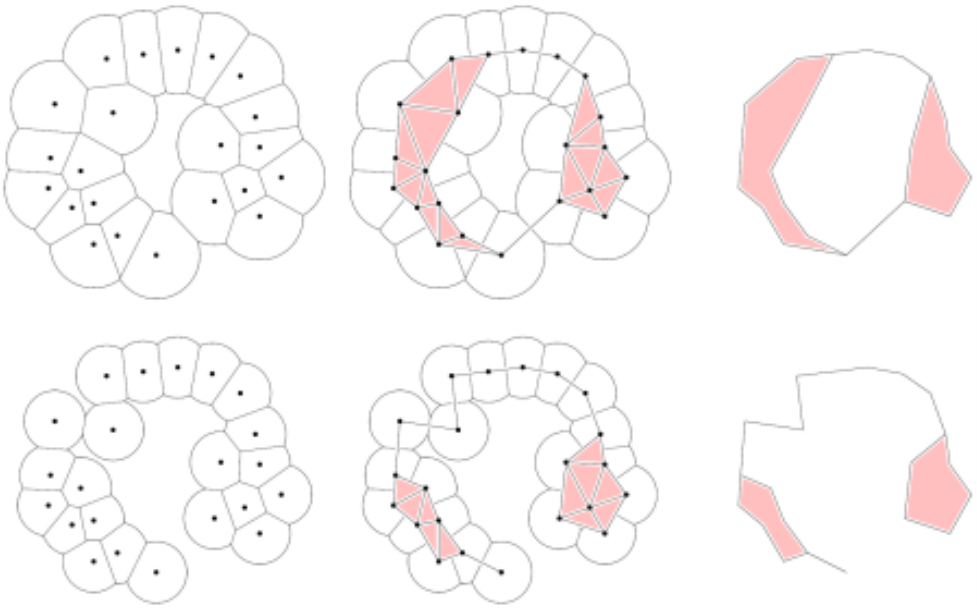

Figure 12: The creation of the Alpha Complex from a set of points. The top row has a larger radius α than the bottom row, providing a different subcomplex of the Delaunay Complex (Van de Weygaert et al. 2011).

3.2 Watershed Transform

A way to identify voids is to apply a watershed transform on a density field. This is based on concepts of mathematical morphology (van de Weygaert et al. 2007).

The morphology of the density field can be described by making an analogy with a mountainous landscape. This image of the density field will have high density 'peaks' and low density 'troughs' with 'ridges' in between. These ridges can be thought of as saddle points. By filling this landscape with water, basins with distinct boundaries will appear. As the water level rises, the boundaries of these basins will change.

This is in principle also how a watershed transform on a density field works. The morphology of the density field will depend on the threshold at which we choose to observe. Before setting a threshold, the image will contain many (local) minima and maxima. As the density threshold increases the areas below will merge into basins. Again, by increasing the threshold the basins will grow and its boundaries will change. This will result in segmentation of the density field into distinct voids, which can be thought of as basins below a certain density threshold. The boundaries and their intersections represent the filaments and clusters respectively.

The watershed void finding technique holds several advantages. For an ideal smooth density field without noise it can be a parameter-free way to identify voids (Colberg et al. 2008). In practice however, we do have to deal with noise and a few parameters have to be introduced to filter out discreteness noise. Filtration of noise can be done by choosing appropriate values for the smoothing and wall parameters, which describe the smoothness of the density field and the minimum density height at the boundaries to either distinguish the area within as separate voids or merge them respectively. The values of these parameters depend on the properties of the data.

Moreover, the voids identified by a watershed transformation may have any shape and strongly reflect the topology of the field. The void boundary is detected even if the boundary is distorted and produces closed contours naturally (Colberg et al. 2008).

Watershed Void Finder (WVF) (Erwin Platen, Rien van de Weygaert & Bernard Jones 2007) is a void finding method based on the watershed transform which is used to identify the structure of the universe in an efficient way. This procedure consists of several steps.

Given a Delaunay Tessellation Field Estimator (DTFE), which defines a continuous density field in a sample volume from a N-Body simulation, the hierarchical nature of the cosmic web and its morphological character can be seen by studying the walls, filaments, clusters and voids in this DTFE image at various density thresholds. The DTFE field is then sampled on a grid, with the size of the gridcell depending on the interparticle separation such that the resolution is high enough to distinguish all the morphological structures. The DTFE field is smoothed by finding the Voronoi cells around each point and by computing the maximum, minimum and median within each Voronoi cell. By doing a uniform partitioning of the cumulative density distribution, the image is transformed into a discrete set of density levels. By smoothing over a pixel radius of 2 (this smoothing will be used in the analysis of voids) the pixel by pixel fluctuations are reduced further. The DTFE field minima are then found by identifying the pixels which are completely surrounded by pixels of a higher density. From these minima the flooding procedure starts with all the pixels below the threshold density being added to the basins. By successively increasing the threshold the basins around the minima will grow. The pixels which are reached by two distinct basins will form the boundary and result in the segmentation of void patches. Finally one may set an extra threshold on the segmentation boundaries (wall parameter), causing voids with boundaries below this threshold to merge into one larger void. The general accepted value for the wall parameter is δ = -0.8 (Platen et al. 2007).

Even though the watershed transform provides us a way to identify, classify and trace voids, it lacks information on the connectedness of the cosmic web and how objects within it react to deformations (Wilding 2018). This can be done by combining the concepts of mathematical morphology and watershed transform with topology.

3.3 Morse-Smale Complex and Persistence

Because the structure of the universe very much depends on the density range in which we choose to observe, features will emerge and die out as we adjust this range. Thresholding changes the morphology of the density field together with its minima, maxima and saddle points. At these critical points the topological structure of the density field can change as we shift the threshold (van de Weygaert et al. 2013).

The evolution of the homology groups, as defined by the Betti numbers, can be displayed by the formation of a torus from a point (see Figure 13 and Figure 14) (Wilding 2018):

1. Starting with an empty space, we add a point (0-Manifold) at the minimum (u).
2. We expand this point which doesn't change the topology.
3. Upon reaching the first saddle point (v) we attach a handle (1-Manifold) creating a tube-shaped object.

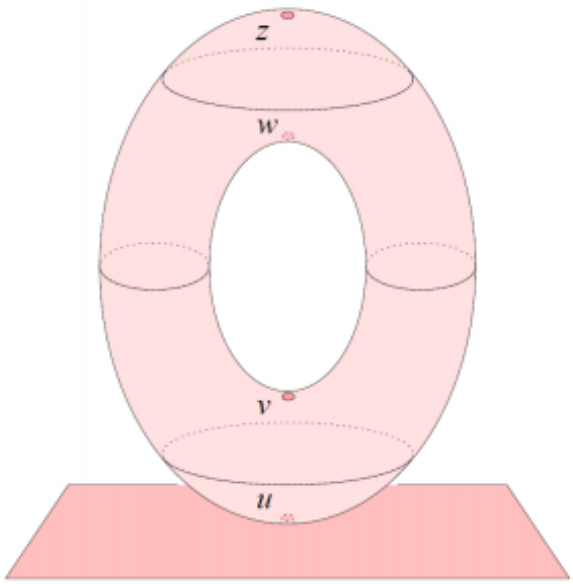

Figure 13: The shape of a torus with the critical points indicated at u, v, w and z (Edelsbrunner and Harer 2010).

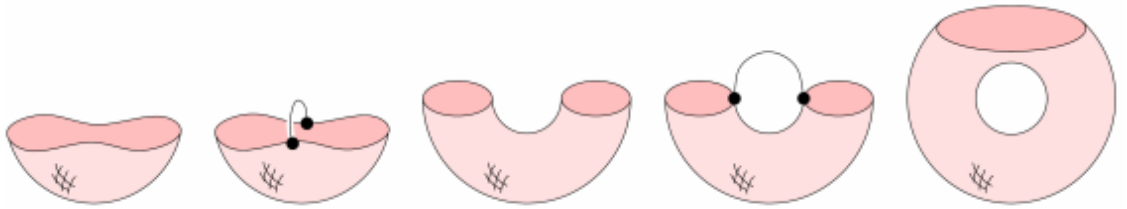

Figure 14: The construction of a torus from a point by adding handles at the saddle points and a disc at the maximum (Edelsbrunner and Harer 2010).

4. Again, we expand without changing the topology.
5. Adding a second handle at the next saddle point (w) creates a loop in the center.
6. Continue expanding.
7. Upon reaching the maximum (z) we add a disc (2-Manifold) to enclose the object, creating a torus.

From the steps above we conclude that the topology changes by adding elements like a point, a handle or a disc at the critical points. Each element has a boundary which corresponds to the boundary of a specific part of the torus. Adding a point increases the zeroth order Betti number β_0, adding a handle increases the first order Betti number β_1 and adding a disc increases the second order Betti number β_2. So after going through all the steps described above, we eventually end up with a set of Betti numbers that correspond to a torus ($\beta_0 = 1, \beta_1 = 2, \beta_2 = 1$). Each set of β_0, β_1 and β_2 determines which homology group the object belongs to (Edelsbrunner & Harer 2001). Because the distribution of the critical points depends on the multiscale structure of the cosmic web, they will emerge and die out by shifting the density threshold in which we choose to observe. This is the very essence of persistent homology which describes the persistence of connected clusters, loops and voids in the cosmic web.

Next we can have a brief look at the mathematical description of the Morse-Smale complex (Milnor

1963) which leads to the notion of persistence. From the collection of critical points we can define the Morse function on a Manifold, $h : M \rightarrow R$, such that:

(i) all critical points are non-degenerate, and
(ii) the critical points have distinct function values.

Now we can construct path integrals (γ) on the manifold M with maximal path p whose tangent vectors agrees with the gradient of the manifold. Integral Lines have the following properties:

(i) Any two integral lines are either disjoint or the same.
(ii) Integral lines cover all of M.
(iii) The limits are critical points of h.

Next, we can distinguish between stable and unstable manifolds. A stable manifold (descending manifold) of a critical point u of h is the point itself together with all regular points whose integral lines end at u. An unstable manifold (ascending manifold) of a critical point u of h is the point itself together with all regular points whose integral lines originate at u.

We can define the Morse-Smale function to be a Morse function, $h : M \rightarrow R$, whose stable and unstable manifolds intersect transversely.

By intersecting all stable and unstable manifolds we obtain Morse cells (see Figure 15). For 2-Manifolds, all minima and maxima are connected to two saddle points and all saddle points are connected to two minima and two maxima (Edelsbrunner & Harer 2001).

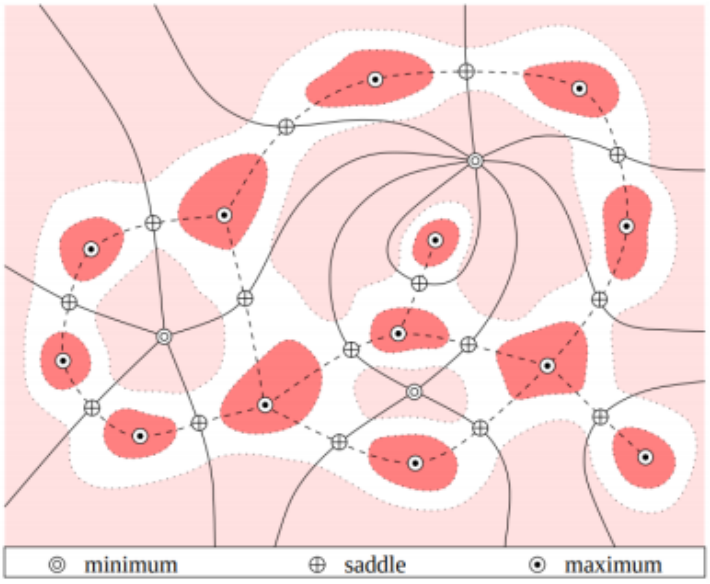

Figure 15: A collection of Morse Cells forming the Morse-Smale Complex (Edelsbrunner and Harer 2001).

We can distinguish the cells into three categories. Cells of dimension 0, 1 and 2 correspond to vertices, arcs and regions, respectively. Each vertex is a critical point, each arc is half of a stable or

unstable 1-manifold, and each region is a component of the intersection of a stable and an unstable 2-manifold. The Morse-Smale complex is the collection of all Morse cells (Edelsbrunner & Harer 2001). The way it is constructed from a density field is shown in Figure 16.

The Morse-Smale complex can be used to determine the persistence of critical points by pairing them up. The persistence can then be defined as the distance between one critical point and its paired critical point, where the pairing is done by coupling a point of creation with a point of destruction. A Critical point is called positive when a topological feature is created. A negative critical point then corresponds to the destruction of a topological feature (Edelsbrunner & Harer 2001).

3.4 Application to the Cosmic Web

To provide some clarification of this abstract mathematical description: in the context of the cosmic web topological features represent either connected clusters, loops or voids.

We can apply this pairing of critical points to each of the three Betti numbers β_0, β_1 and β_2 in a density field of the cosmic web. These will be called Birth-Death pairs and their distance depends on the morphology of the density field as a result of a chosen threshold density.

Dimension 0: The maxima can be a positive critical point leading to the creation of connected components, increasing the value of the zeroth order Betti number β_0. The connected pair then corresponds to a saddle point with index 2. At this saddle point the destruction of connected components occurs which decreases the value of β_0. The index refers to the number of eigenvalues which is correlated to the number of independent directions where the field decreases, meaning there are 4 distinct classes of critical points: maxima with index 3, saddle points with index 2, saddle points with index 1 and minima with index 0.

Dimension 1: Moving up one dimension we can pair saddle points of index 2 with saddle points with index 1, leading to the birth and death of loops respectively. This changes the first order Betti number β_1.

Dimension 2: The birth and death of voids is described by pairing up saddle points with index 1 with minima. This changes the second order Betti number β_2.

A persistence diagram (see Figure 14) can be made by comparing the threshold value at which a certain feature is born and at which a certain feature dies (Pranav et al. 2017). They provide a useful way to filter out noise from our data-set, which often corresponds to very short-lived features (van de Weygaert et al. 2013). But more importantly, it serves as a way to distinguish the persistent features of the cosmic web (Wilding et al. 2021) .

Persistence diagrams can be applied not only to the density field, but also to the velocity field and the gravitational potential. Persistent topology together with the watershed transform will provide a rich analysis of the overall structure and dynamics of voids.

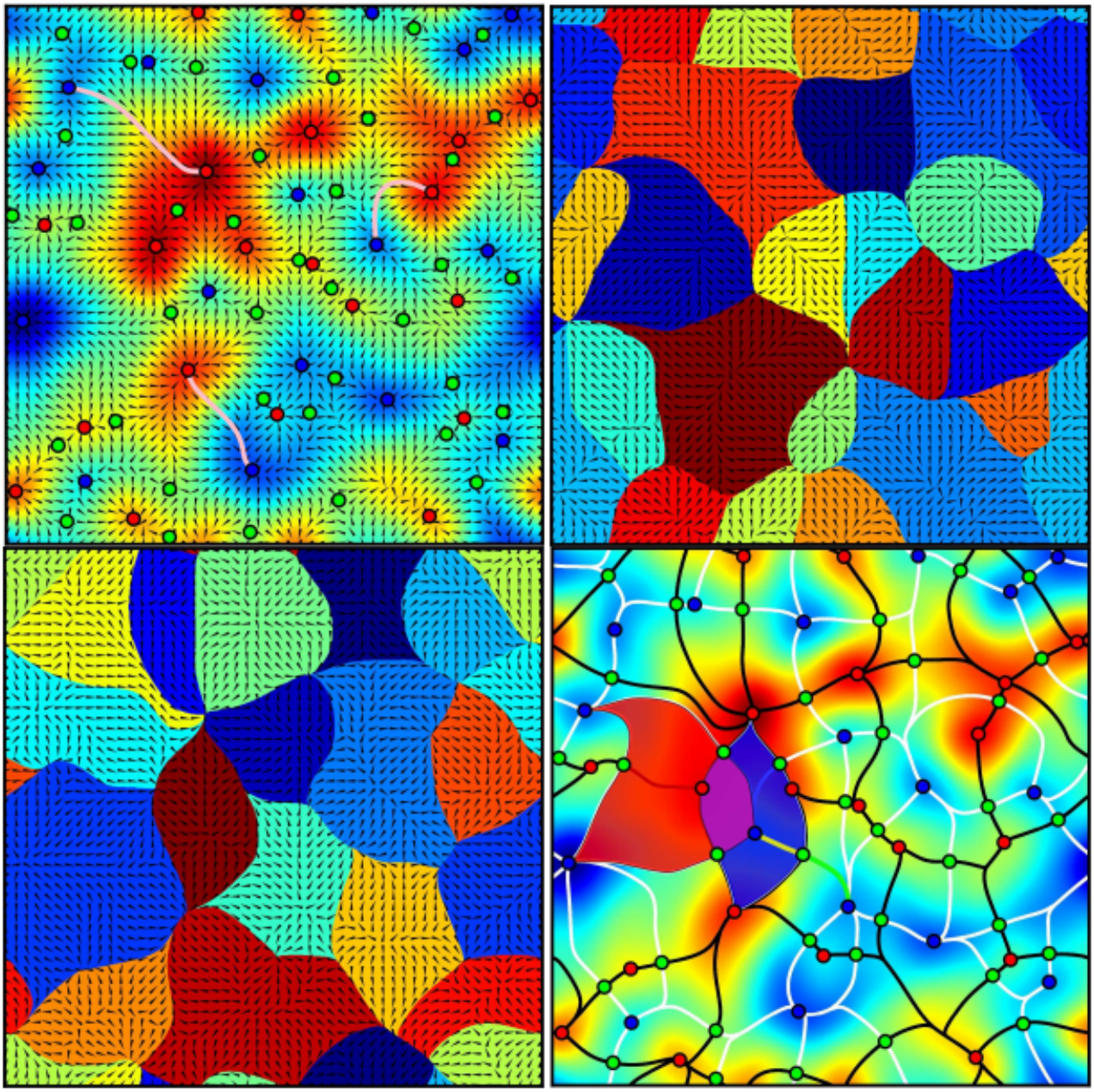

Figure 16: Top left panel shows a two-dimensional density field with its gradient and some of the path lines along the gradient. Top right shows the stable (descending) 2-manifolds with the direction of the gradient imposed on it. Bottom left shows the unstable (ascending) 2-manifolds. Bottom right shows the Morse-Smale complex, where the black and white lines correspond to the boundaries of the ascending and descending 2-manifolds respectively. The maxima, minima and saddle points correspond to the red, blue and green points respectively. The purple patch represents the intersection of a red descending 2-manifold and a blue ascending 2-manifold. The Morse-Smale complex is then described by the critical points and lines (black and white). The lines form the arcs, linking the critical points (Sousbie 2010).

4 Results I: Void Hierarchy

4.1 Density Field Filtration

We apply our analysis on the DTFE density field. A slice through the three dimensional simulation can be seen in Figure 17 on a 256^3 grid. The simulation is using 256^3 dark matter particles, each with a mass of $0.443 \cdot 10^{10} M_\odot$ in a box of 300 Mpc. The density is given in ρ/ρ_u, which cannot be smaller than zero. Here a logarithmic scale is used for better visualization. We can clearly see the web-like structure and the presence of clusters, filaments and voids in between. The hierarchical build-up of its features for different density thresholds are evident as well (see Figure 18). From top left to bottom right we see the separated components connecting as the density threshold decreases, eventually leading to the emergence of the cosmic web in the third panel. In the first panel (top left) the density threshold is so high, only the most dense clusters are visible and the structure consists of separated components. As the threshold decreases and the components connect, closed loops and voids emerge. Finally the threshold is met where only underdense separated structures (voids) enter the picture (bottom right).

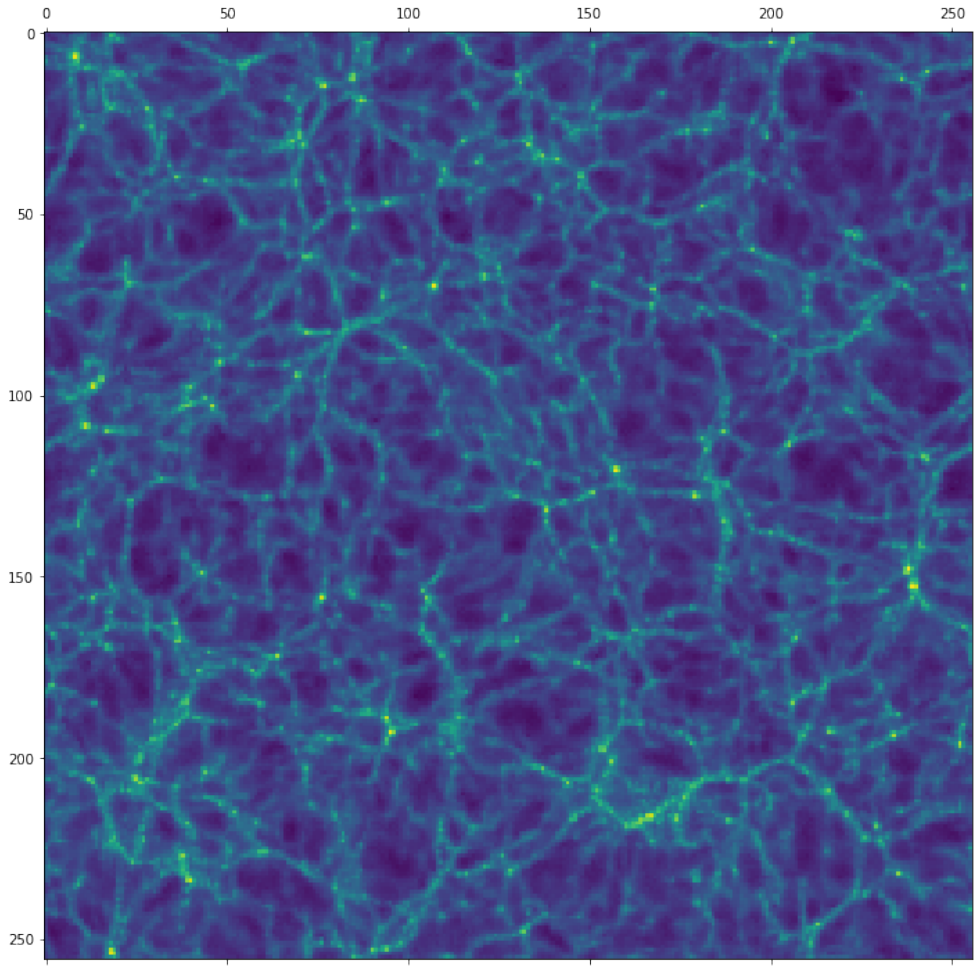

Figure 17: The DTFE density field, displaying the components of the cosmic web (filaments, clusters and voids in a box of 300 Mpc.

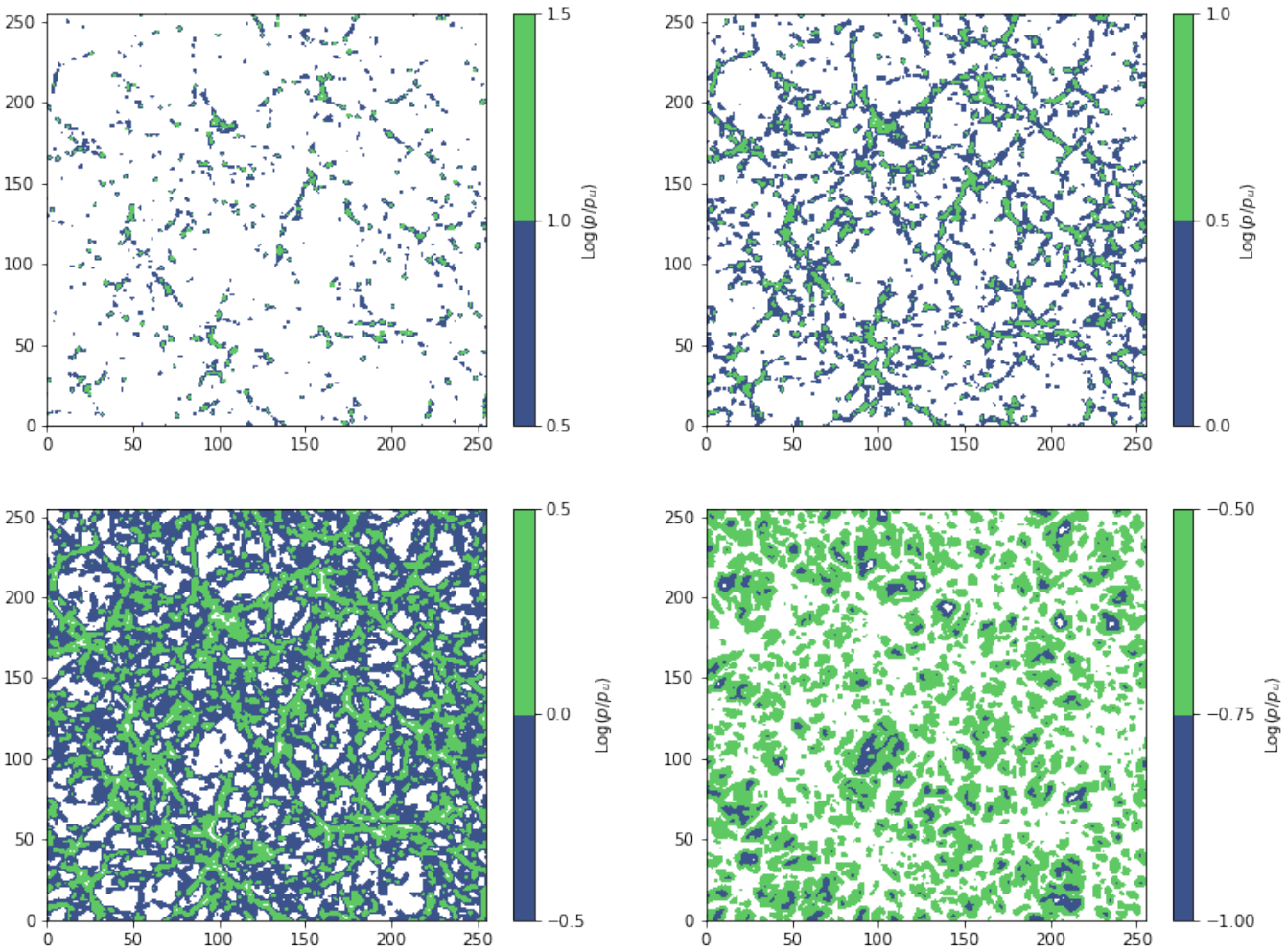

Figure 18: The hierarchical structure of the density field as a result of different thresholds. Here (from top left to bottom right) the transition from clusters to filaments to walls to voids is illustrated. Box length 300 Mpc.

4.2 Watershed Transform versus Morse-Smale Complex

Starting from the density field, we used two ways to proceed with the analysis of voids. First a watershed transform has been applied to the density field to identify the voids. Then we compare the results with a more sophisticated way of finding the voids through the Morse-Smale complex by determining local minima, maxima and saddle points. The voids are then identified by finding the absolute height between their birth at a local minimum and their death at a saddle point. This is also directly related to their persistence. So by using the Morse-Smale complex we are able to identify the hierarchy of voids and get a notion of their persistence at the same time (see Figure 19). Comparing slices of both methods in Figure 20 we can see that the voids identified by the topological analysis of the Morse-Smale complex don't cover all of the box - there are gaps in between.

4.3 Watershed Comparison

Slices of the result from WVF on this density field can be seen in Figure 21. Patches in each image correspond to a separate voids. Various wall parameters (w) and smoothing parameters (r) are

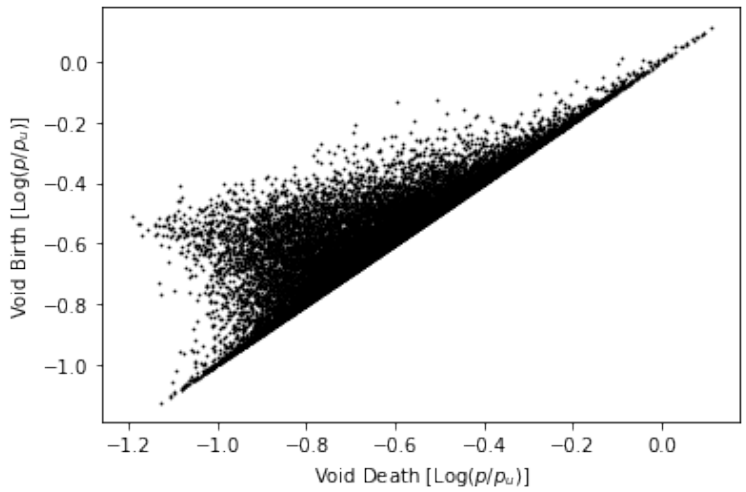

Figure 19: A β_2 persistence diagram describing the creation and destruction of voids. The values on the y- and x-axis correspond to the values for ρ/ρ_u where shells are closed (void born) and filled (void dies), respectively.

used to display their effect at redshift zero. The wall parameter causes neighboring basins with a minimum boundary height below the threshold to be merged. A very low boundary threshold generates oversegmentation, which is visible for w = -1.0 with r = 1. As the threshold for the boundaries between the basins rises, more and more voids will merge. This is clearly visible as the dark-blue patches grow as the wall parameter increases. The smoothing parameter r defines the number of grid cells over which the watershed transform is averaged, creating a smoother image. A higher value for the smoothing parameter provides a less noisy image, as can be seen going from the top to bottom row.

The optimal values for the parameters are w = -0.8 and r = 2, whereas a lower value for w shows a noisy image making it difficult to distinguish the voids. The natural threshold for the wall (w = -0.8) and a smoothing radius of 2 grid cells (r = 2) will be used for the watershed analysis as well as the Morse-Smale complex analysis of the sizes and shapes of voids.

4.4 Void Shapes

After obtaining the void distribution from WVF and TDA through the Morse-Smale complex of the DTFE density field, we can study the shape of each void. Each method will provide a group of grid cells corresponding to a void in the distribution. Assuming the density is uniform within the voids we can fit an ellipsoid to estimate their shape and volume. An ellipsoidal fit to the volume of voids is a decent first-order approximation for its interior as voids are known to have a roundish shape van de Weygaert et al. (2012). Near the fringes of the void the approximation breaks down because of the tidal forces of its exterior.

First, the geometric centre of the void is determined by taking the average of the void's grid cell positions. The void's volume will then simply be the sum of all the grid cells multiplied by the volume of one grid cell. The size of one cell corresponds to a length of (300/256) Mpc. Once we have the geometric centres we calculate the inertia tensor of each void as follows:

$$I_{ij} = \sum_k (\delta_{ij}\vec{x_k}^2 - x_{ki}x_{kj})$$

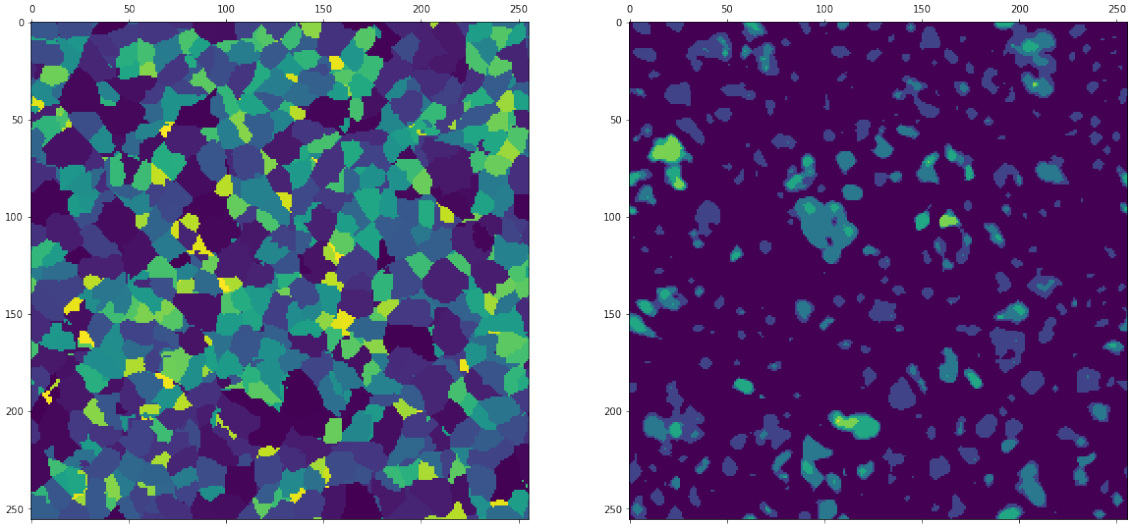

(a) Comparing results WVF and TDA

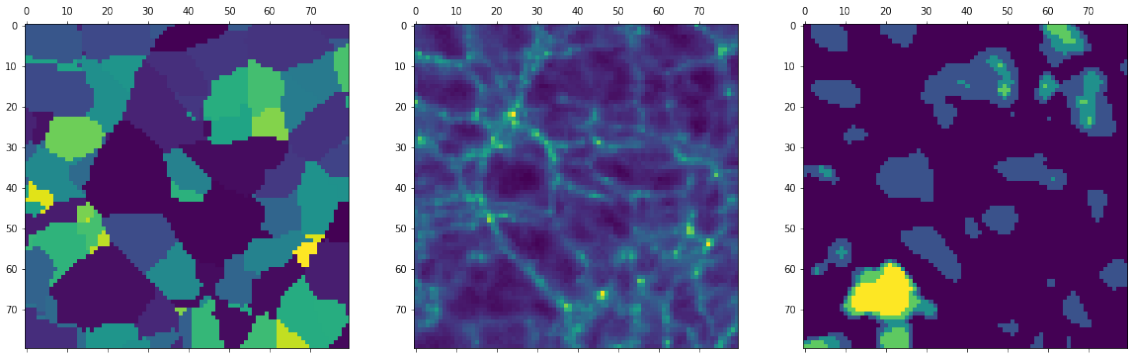

(b) Comparing results WVF and TDA with the density field

Figure 20: A comparison between the voids obtained by WVF (top left panel) and by analysing the critical points in the Morse-Smale complex (top right panel). The patches correspond to voids. In the top right panel nested voids can be seen. The bottom row compares, from left to right, the watershed transform with the density field and the voids identified by the Morse-Smale complex analysis. Box length 300 Mpc.

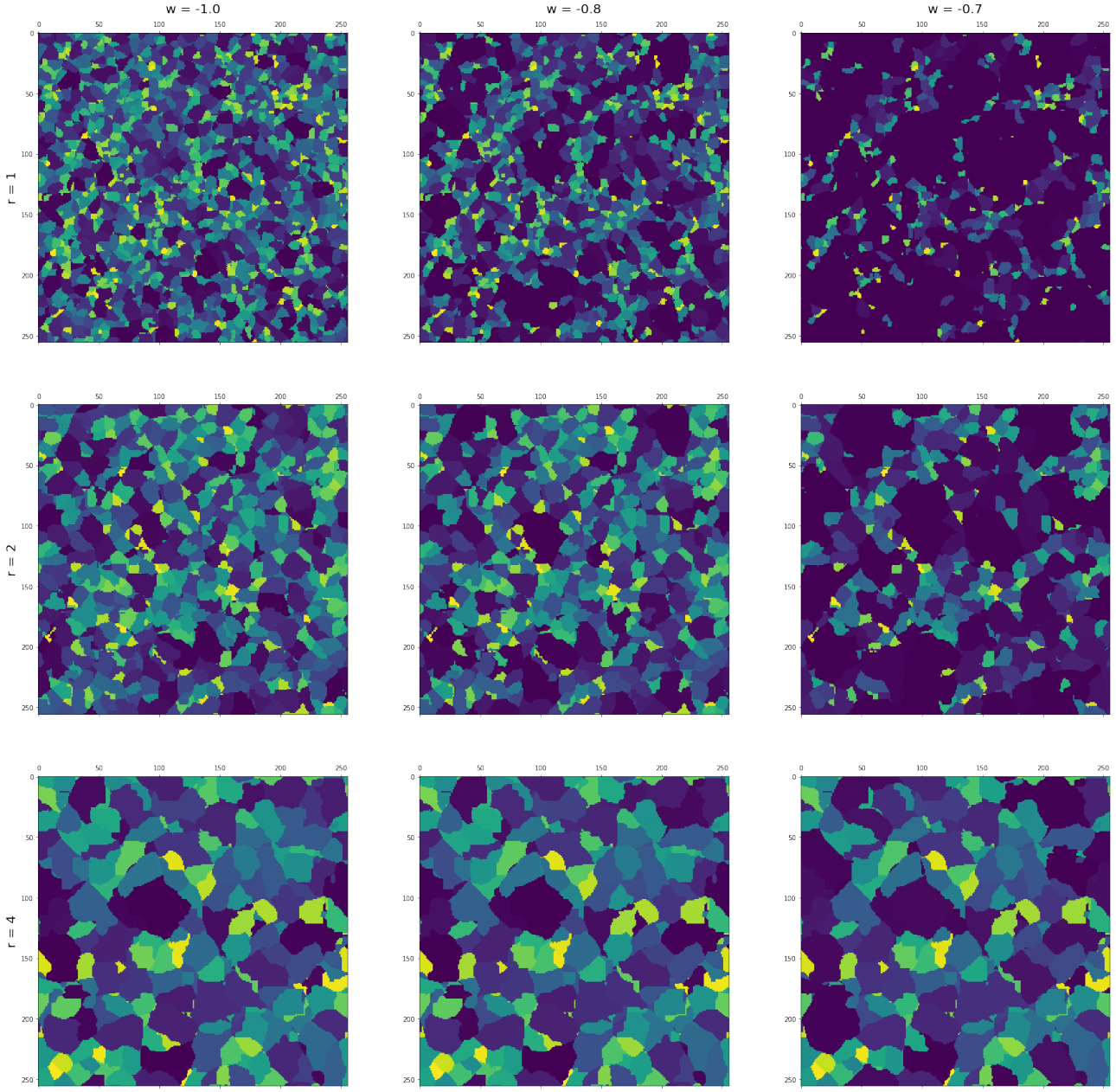

Figure 21: Comparison of different WVF parameters (smoothing parameter r and wall parameter w). As the smoothing parameter rises (from top to bottom) the smoothing radius over the pixels becomes larger and therefore the patches (identified voids) become bigger. As the wall parameter increases (from left to right) more voids will be merged, also leading to the appearance of larger voids. Box length 300 Mpc.

For each void we sum over all void cells k and $\vec{x_k} = (x_{k1}, x_{k2}, x_{k3})$ is the distance vector of the k-th grid cell from the geometric centre. δ_{ij} is the Kronecker delta. The inertia tensor allows us to fully extract the geometric properties of the homogeneous ellipsoids. We choose the ellipsoid with the same inertia tensor as the void as the best fit. The eigenvalues of the inertia tensor correspond to the parameters that determine the shape and orientation of the ellipsoid. The semi-axes of the ellipsoid depend on the eigenvalues as follows:

$$a^2 = \frac{5}{2}(I_2 + I_3 - I_1)$$
$$b^2 = \frac{5}{2}(I_3 + I_1 - I_2)$$
$$c^2 = \frac{5}{2}(I_1 + I_2 - I_3)$$

The parameters are then characterized as: $e = 1 - \frac{c}{a}$, $s = \frac{c}{a}$, $p = \frac{b}{a}$ and $q = \frac{c}{b}$. Where e is the ellipticity, s is the sphericity, p is the oblateness and q is the prolateness. s defines how much a spheroid resembles a perfect sphere ($s = 1$). e defines how much the spheroid deviates from being a perfect sphere. p and q show how much the sheroid is flattened, resembling an oblate or prolate sheroid respectively. The volume of the void will then be V = $\frac{4}{3}\pi r^3$, where $r = \sqrt{abc}$ is its effective radius. Of course the volumes of the ellipsoids will differ slightly from the volume of the voids by counting the interior grid cells, but it is a decent estimate. A slice through the three-dimensional ellipsoid fits are shown in Figure 22 as ellipses.

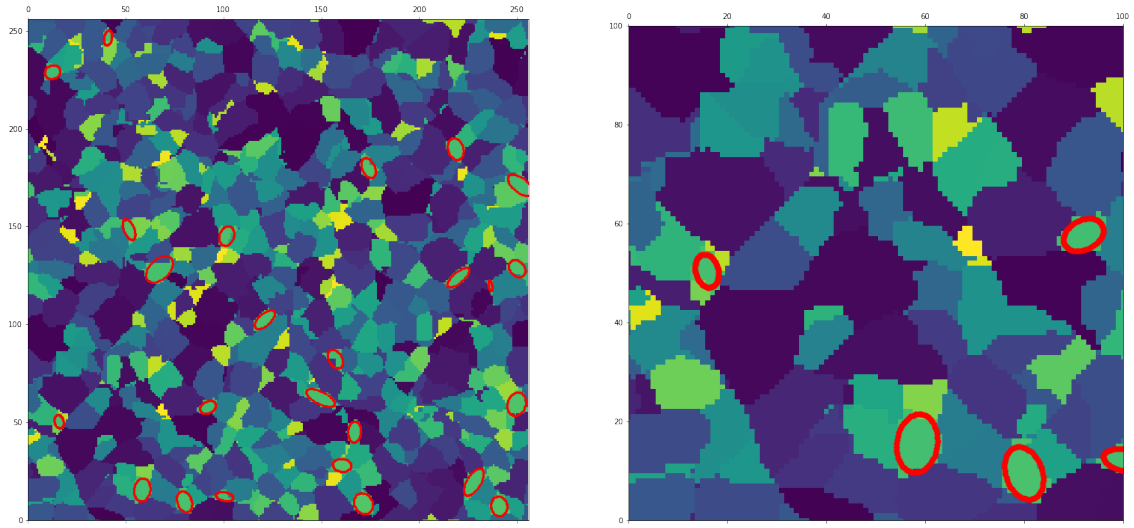

(a) (b)

Figure 22: A slice through the ellipsoidal fits to voids. The right panel zooms in on the left bottom corner. Box length 300 Mpc.

Comparing the PDF's of the shape parameters (Figure 23) found by the watershed analysis and the ones found through the Morse-Smale complex, we don't see a clear difference. The functions look similar with peaks at approximately the same values for each shape parameter, even though there is a slight shift of the sphericity towards 1 for the TDA voids compared to the WVF voids (which means they tend to be a little bit more spherical). Considering the voids found through topological analysis (TDA), there is a peculiar shape to be seen in the distribution when plotting the shape parameters against the volume of the fitted ellipsoids (Figure 25). Especially considering the sphericity and prolateness of the voids, the small voids are very much clustered with values ranging from 1 to $10^{-0.3}$ and from 1 to $10^{-0.1}$ respectively. This implies small voids tend to be very close to a perfect sphere. This result might be questionable. The resolution of the grid causes a less accurate prediction of the shapes of smaller voids compared to the larger ones. The spreading keeps growing for larger void

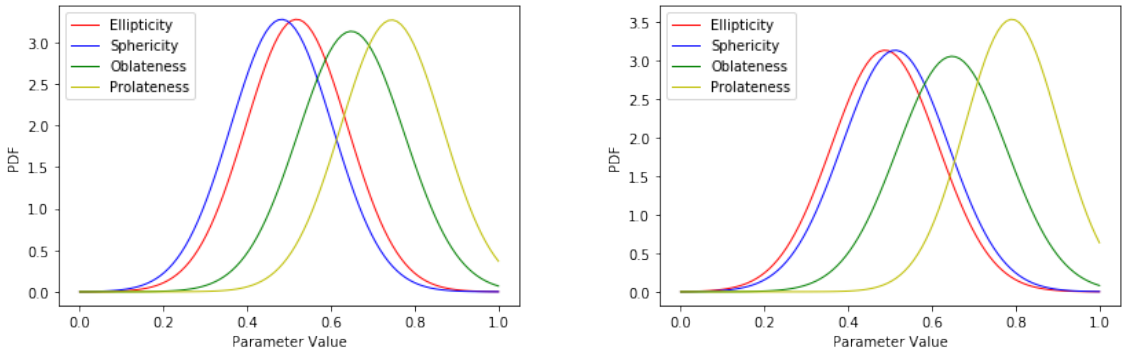

(a) WFV (b) TDA

Figure 23: The PDF's of the shape parameters of voids.

volumes. This trend is not seen in the watershed analysis (see Figure 26). In contrast to WVF, TDA allows nested voids which results in a higher abundance of smaller-sized voids. In WFV these nested voids would be part of a larger void instead. One big advantage of the topological (Morse-Smale complex) approach is that it can relate the different void shapes and sizes and their persistence. As can be seen from Figure 25, persistent voids have a larger volume and have a larger spread in the distribution of the parameters. The smaller voids are more clustered, less persistent and have a higher abundance (see Figure 24).

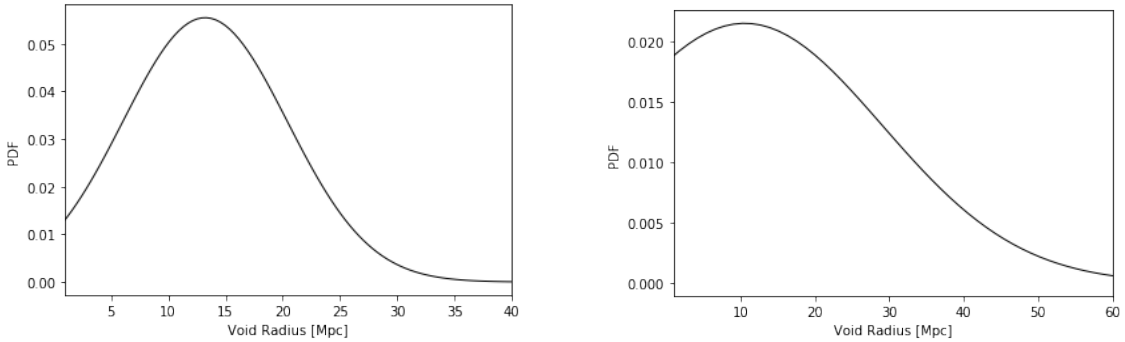

(a) WFV (b) TDA

Figure 24: The PDF's of the raddii of the ellipsoids fitted to the voids. The voids found by WFV peak at a larger radius compared to the voids identified via TDA.

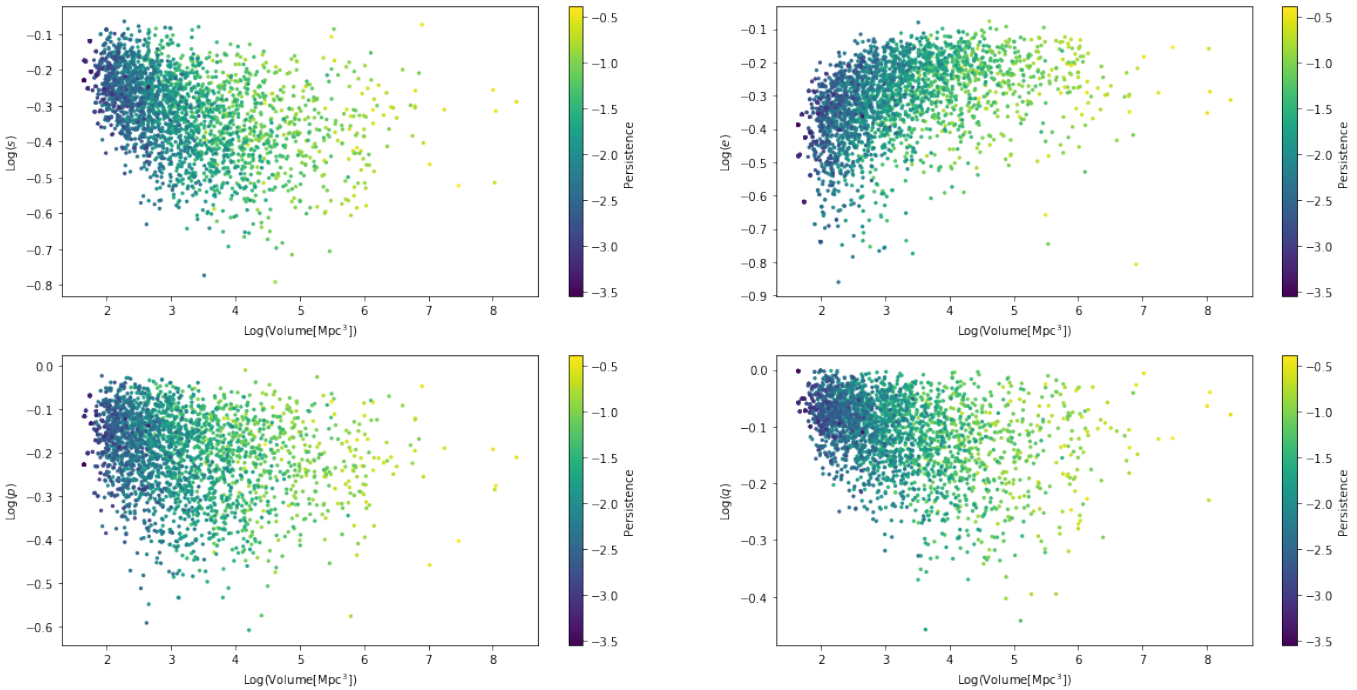

Figure 25: Comparing the shape parameters of the voids found through the Morse-Smale Complex with the fitted ellipsoid volumes. The colorbar indicates the corresponding persistence which is defined as Log(Birth[Log(ρ/ρ_u)]-Death[Log(ρ/ρ_u)]). Yellow is high persistence, blue is low persistence.

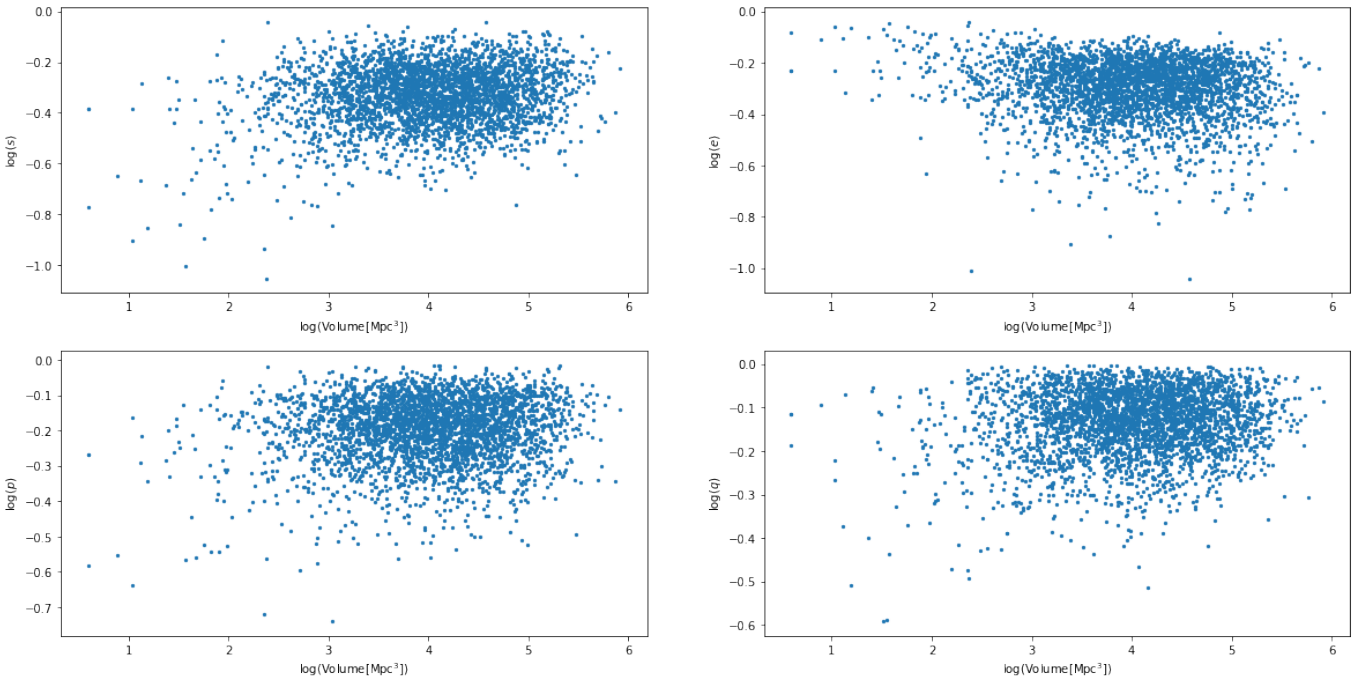

Figure 26: Comparing the shape parameters of the voids found through the watershed analysis with the fitted ellipsoid volumes.

5 Results II: The Topology of the Potential Field

5.1 Gravitational Potential

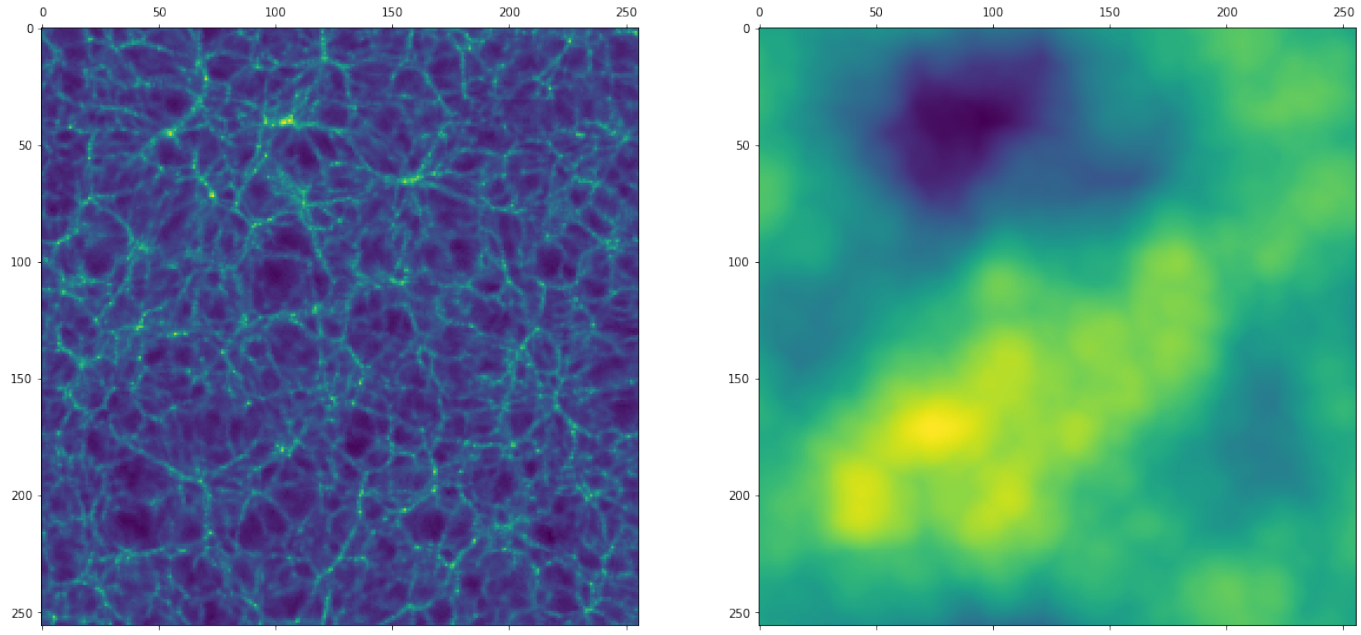

Figure 27: In the left panel the DTFE density field and in the right panel the corresponding gravitational potential field. The dark blue potential well corresponds to the cluster in the upper left of the field. Matter follows the gradient towards this cluster. The bright yellow peaks in the potential correspond to the low-density regions in the density field. The blue potential wells in the right panel tend to follow the filaments and clusters in the left panel. Box length 300 Mpc.

From the density field we may proceed to find the corresponding gravitational field. The Poisson equation will allow us to make such a transformation:

$$\nabla\phi = 4\pi G\rho$$

The solution of the gravitational potential ϕ can then be found by integrating over the Green's function:

$$\phi(\vec{x},t) \sim \int \delta(x') \frac{1}{|x'-x|} dx'$$

Where the the integral is taken over the co-moving space x', and $\delta(x')$ is the density fluctuation.

Another way to write this down is in terms of the density field and its Fourier decomposition:

$$\phi(\vec{x},t) \sim \int \frac{1}{(2\pi)^3} \frac{1}{k^2} \hat{\delta}(k) e^{-i\vec{k}\cdot\vec{x}} dk$$

Where $\vec{k}$ is the wave vector, $\hat{\delta}$ is the amplitude of the wave and $\vec{x}$ is the position in the density field. The relation between the amplitudes of the density and potential Fourier decompositions is then:

$$\hat{\phi}(k) \sim \frac{1}{k^2} \hat{\delta}(k)$$

It shows that the density spectrum is more sensitive to the small-scale density field (10 to 25 h^{-1} Mpc) van de Weygaert (2005), while the potential spectrum is more sensitive to large-scale fluctuations. The amplitude of the wave from the potential Fourier decomposition $\hat{\phi}$ is less dominated by high frequencies (large k), which results in a smoother appearance of the gravitational field compared to the density field. The potential looks more 'quiet'.

Applying the Fourier transform to each grid cell of the density field returns a gravitational potential field on a 256^3 grid (Figure 27). Comparing different slices through the three-dimensional space of the density and potential, we notice the voids correspond to peaks and clusters to troughs in the gravitational field. This should be the case, because streams of matter flow out of the underdense voids to the overdense clusters as a result of gravitational attraction.

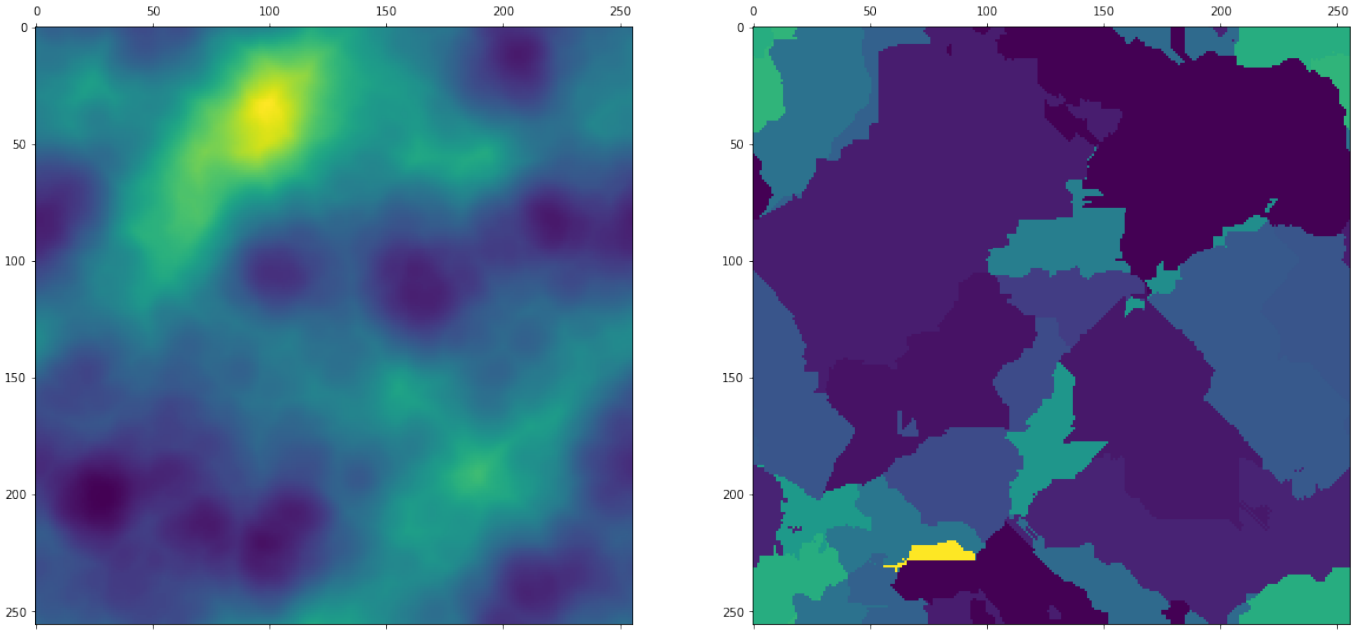

Figure 28: In the left panel the reversed gravitational potential and in the right panel the result of WVF. Here the bright yellow spot forms the maximum in the reversed potential field and corresponds to the cluster in the density field, while the dark blue spots form the minima corresponding to the low-density regions in the density field. Box length 300 Mpc.

The appearance of peaks and troughs in the potential makes it appealing to provide the same watershed analysis on it, as we have done for the density field. To be able to run WVF on the potential it has to be reversed, such that the peaks correspond to the clusters and the troughs to the voids. However, the result of WVF on the gravitational potential is not fulfilling the expectations (see Figure 28). The patches in the watershed image should match the troughs in the reversed potential, which is not the case.

5.2 Persistence

Now we have the density field and its corresponding potential, we might as well look into their topological features through persistent homology. A persistence diagram can be made by determining for

which values in the density and potential field independent features are born and die out. The three Betti numbers β_0, β_1 and β_2 then count the number of independent features. β_0 identifies the number of separate components, while β_1 and β_2 correspond to the number of loops and the number of enclosed spaces respectively. While comparing the persistence diagrams of the density and potential, they show a difference in the number of Birth-Death pairs (see Figure 29). There are far less critical points in the gravitational field. The topological features in the potential seem to be not persistent at all, because all the Birth-Death values are very close to the diagonal. The persistence diagram of the density field shows a richer variety in persistence of separated components, loops and voids. Looking at the potential field using various thresholds, one might notice less features while comparing it to the density (see Figure 30 and Figure 18).

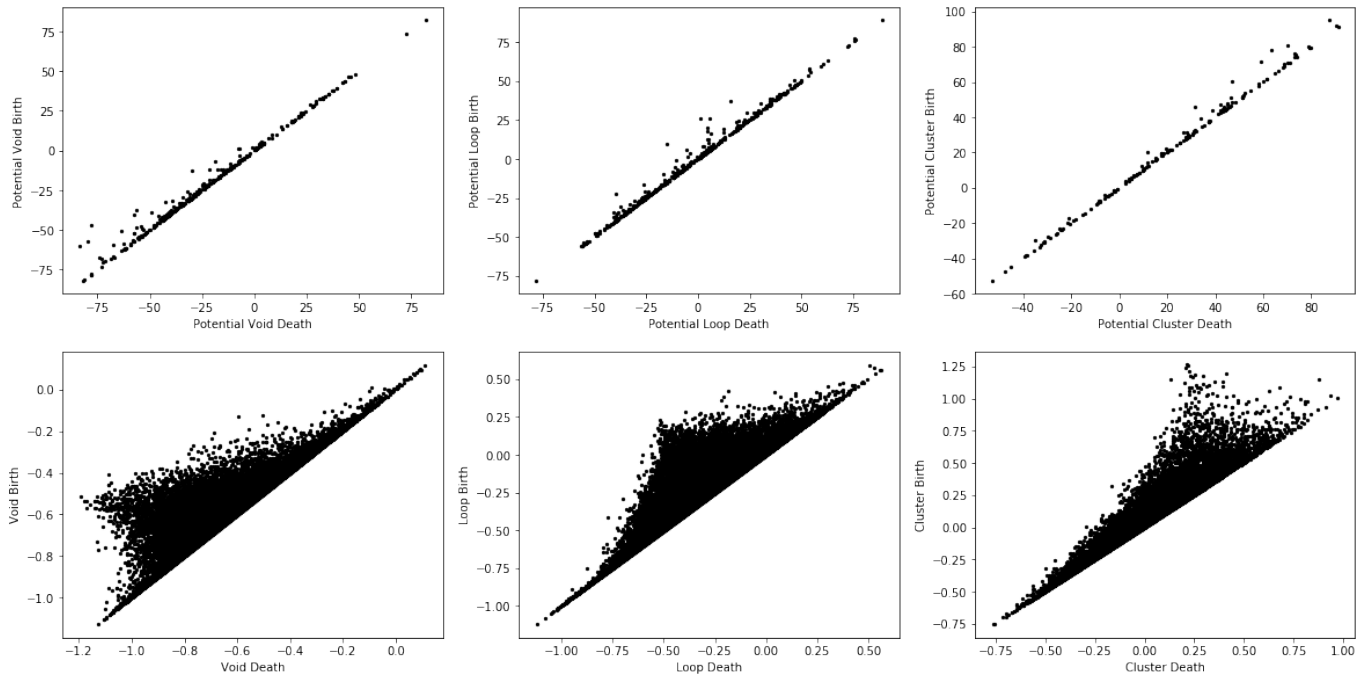

Figure 29: A comparison between the persistence diagrams: potential vs density. They show for which potential field height (top row) and density (bottom row) different features are born and die. The densities on the x- and y-axis in the bottom row are given in $\mathrm{Log}(\rho/\rho_u)$. The x- and y-axes in the top row correspond to the potential height (without taking into account the proportionality constant).

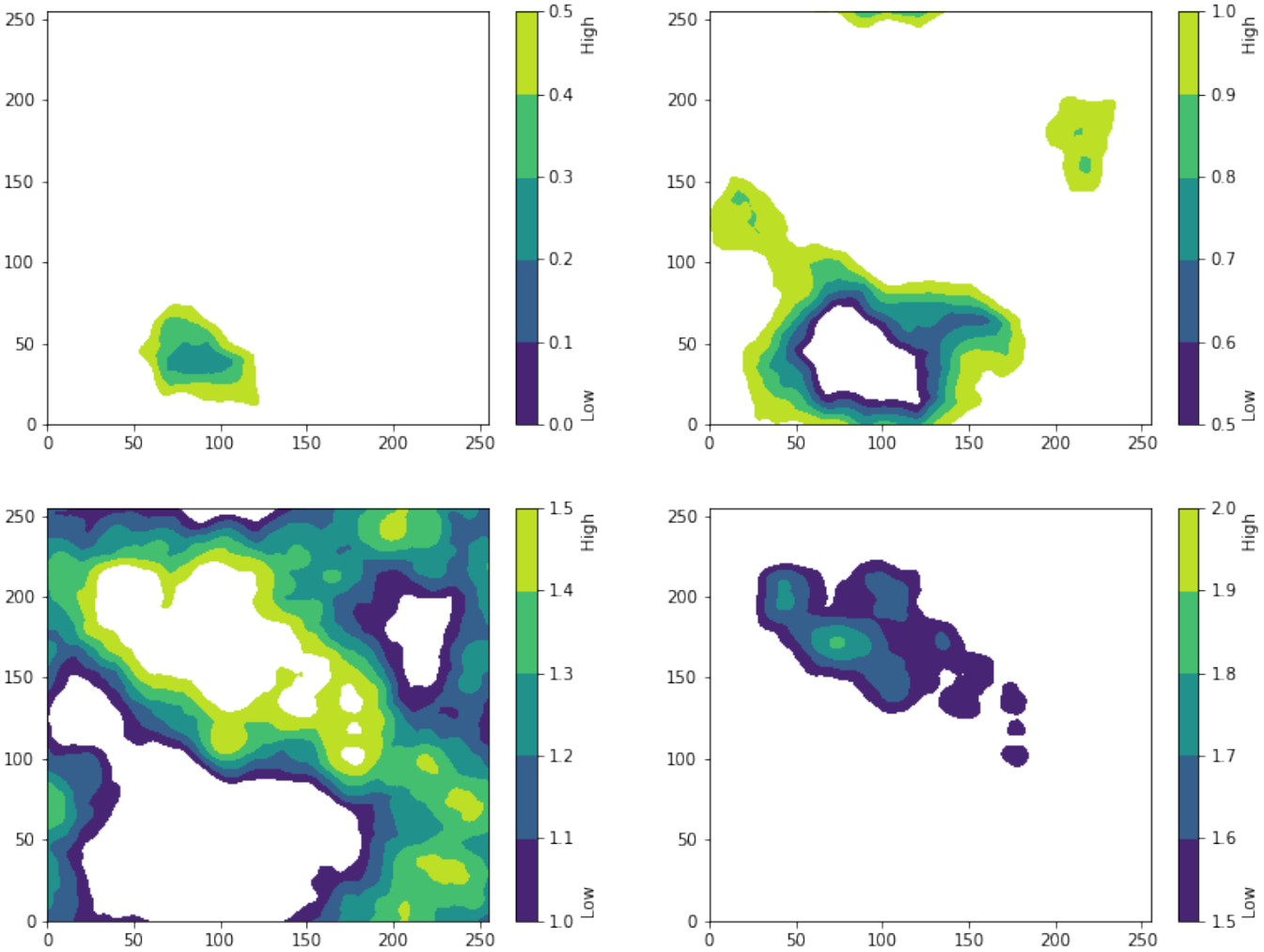

Figure 30: Showing the features of the reversed gravitational potential field (rescaled) for different thresholds. It has a less rich structure compared to the density field. Box length 300 Mpc.

6 Conclusion

6.1 On WVF and the Potential

Clearly the result of WVF on the gravitational potential didn't meet the expectations. The basins in the watershed transform do not match the troughs in the reversed potential. Difficulties might arise when applying a watershed transform on the DTFE density field and its corresponding potential field. The filaments don't necessarily correspond to the boundaries of the void patches, because they do not comply with the Morse criterion: the field lines (integral lines) might cross on locations other than the critical points, leading to spurious intersections (Sousbie 2010). Because of this, the boundaries of the watershed transform of the density field do not always match the presence of filaments. Figure 31 is an illustration of the problem of finding the Morse-Smale Complex from a non Morse function when using a watershed based method, comparing the two- and three-dimensional case (left and right panel respectively).

The left panel shows the filaments (black lines) forming a pseudo Morse-Smale complex (a network that links the critical points together) with the the gradient direction along these lines (grey arrows) of a two-dimensional desnity field sampled at discrete locations. The maxima, minima and saddle points are shown as red, blue and green points respectively. The letters indicate the different regions enclosed by the filaments. Zooming in on one of the vertices shows that the lines cross at a location where no critical point is present, not complying with Morse criterion. If the lines would be consistent with the Morse criterion, they would represent the blue dashed line in the zoomed frame.

The right panel illustrates the filaments identified from DTFE density field simulation (512^3 dark-matter particles in a 50 h^{-1} Mpc box). The surface is shaded according to the logarithm of the density and represents the triangulated interface between the void patches. The red and yellow lines correspond to filaments located at the interface of at least three different void patches found using the watershed method. A dark-matter halo is present in the centre-right part of the image. The yellow line is spurious because it doesn't correspond to locations of overdensity in the field.
Real filaments would pass through the local maximum (the centre of the dark-matter halo), while the network of the red and yellow lines don't. By shifting the red line to the blue dashed line and removing the misleading yellow line it would represent a more sensible network of filaments. This error is similar to the two-dimensional case, caused by the lines not being compliant to the Morse criterion. The little sketch in the left corner shows what happens along the black dashed line. In the plane perpendicular to the surface two void patches (A and B) are being squashed by two other voids patches (C and D). Two spurious intersections are indicated by the red dots, while the real critical line is indicated by the blue dot (where the four patches truly intersect).

While WFV is an efficient way to locate voids within the Cosmic Web, its results aren't very reliable when it comes to defining their proper exterior (filaments), according to Sousbie (2010). The deviations, when comparing the boundaries of the watershed transform and the filaments in the DTFE density field, are more prominent in three dimensions (Sousbie 2010). In the same way, the result of WVF on the gravitational potential field might deliver unexpected boundaries. The errors in the watershed result on the potential might be enhanced because the field is extra smooth, leading to more spurious intersections and eventually showing boundaries that don't make sense. If this is the case, these limitations of the watershed based method would push us to find another method which is consistent with the Morse criterion.

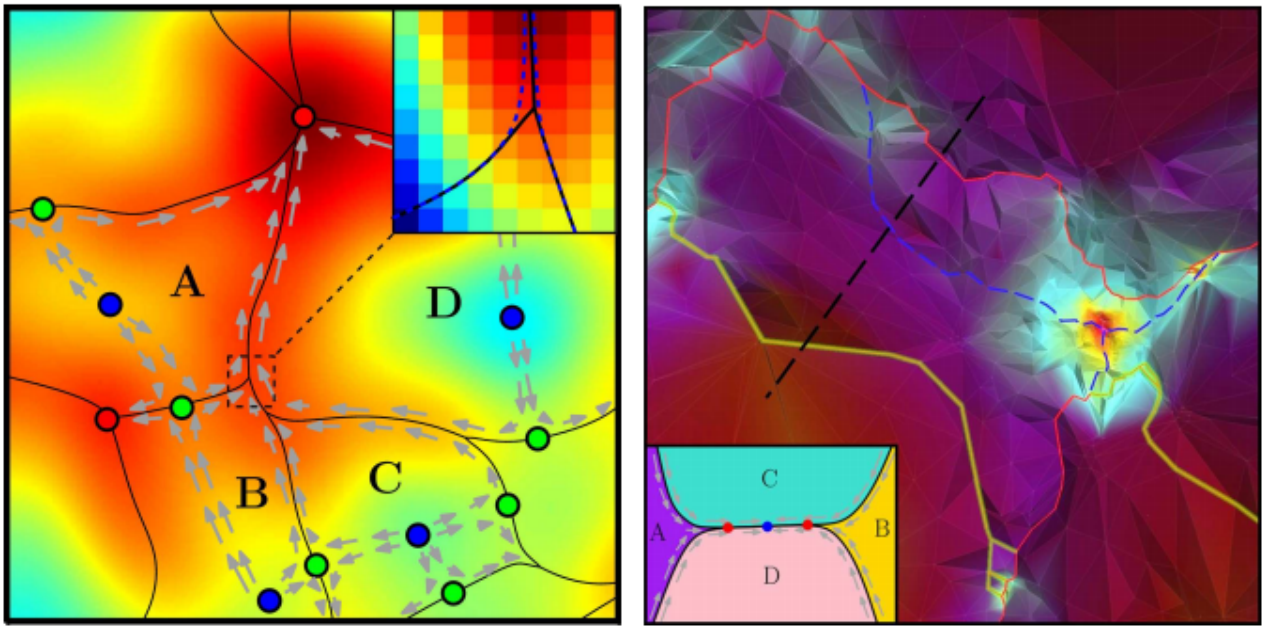

Figure 31: Illustration of the problem of finding the Morse-Smale Complex from a non Morse function when using a watershed based method (see main text for a more thorough explanation). (Sousbie 2010).

Another explanation for the unexpected result of WVF on the potential field might reside in the Fourier decomposition of the potential and the relation between the power spectra of the density, velocity and potential field:

$$P(k) \sim k^2 P_v(k) \sim k^4 P_\phi(k)$$

Because the potential spectrum is less sensitive to small-scale fluctuations, the wall threshold parameter might make the separation of 'potential voids' troublesome. The algorithm of WVF is fine-tuned to detect voids in a density field. The result of DTFE is given in ρ/ρ_u, which is the density divided by the mean density. It is then trivial to convert it to δ which is used to determine the thresholds. However, transforming the density to the gravitational potential makes δ impractical. The -1 in the definition of δ can cause major problems when determining the walls of the watershed transform because the power spectra have a different dependence on the wave vector $\vec{k}$. The potential spectrum is sensitive to large-scale fluctuations while the the density spectrum is susceptible to the small-scale fluctuations. The PDF of the gravitational potential is not entirely Gaussian either. There are not as many Fourier modes in the gravitational potential, which might skew the PDF. Adjusting WVF to the lower frequencies of the Fourier decomposition might solve the problem.

6.2 Issues with the Void Shapes

Regarding the sizes and shapes of voids, identified by WVF and TDA, the difference in the distribution arises for the fact that TDA allows nested voids while WVF doesn't. TDA is a more natural way of probing the hierarchical nature of the void population. There is a more dynamic range of wall-density heights the boundaries can have in the TDA analysis, whereas WVF only uses one predefined wall parameter.

Also, difficulties might arise as the resolution determined by the grid is not enough to define the shapes of smaller voids by fitting an ellipsoid. This method of determining void shapes through the inertia tensor only seems to work for larger voids with well-defined boundaries. For the nested voids we would need a grid with higher resolution and more void-pixels, which will undoubtedly require more computational power.

6.3 Further Research

6.3.1 Ellipsoid Fits

For further research, we might want to repeat this procedure of fitting ellipsoids through voids at various redshifts for different cosmological models. We would obtain the evolution of the shape parameters and expose the void dynamics. The role of dark energy and tidal forces from the void's exterior can be investigated from the observed dynamical effects and reveal which forces are dominant. It would be interesting to see how the void sizes and shapes are affected by different cosmologies, compared to the LCDM model.

6.3.2 Substructure Remnants

We could also look more into the void hierarchy by analysing the merger tree of voids by tracing their connectivity, for instance in the Morse-Smale complex. The fate of the void substructures may be reconstructed with more precision that way. N-body simulations show that voids do retain a rich infrastructure even after it is diminished at an ever decreasing density contrast (van de Weygaert & Platen 2009). These 'leftovers' of the earlier phases of void hierarchy when the substructure was more prominent keep lingering around. The voids mostly retain the topological characteristics of the initial density field. By studying the connectivity through the Morse-Smale complex we could reconstruct some of the history and evolution of these voids.

6.3.3 Velocity Field

So far we have only compared the density fluctuations in the cosmic web and their potential field. By including the corresponding velocity field we will obtain a more complete view of the dynamics of voids and the direction of the outflow of matter towards its exterior. The identification of voids from the density field, the direction of the streams of matter from the velocity field and the range within structures are bound by clusters from the gravitational potential field give, a comprehensive description of the nature of the cosmic web. We can compare the results from simulations, e.g the DTFE density field and its corresponding velocity and potential field, to the velocity flow streams within the Laniakea supercluster (Tully et al. 2014). This way we can check whether the velocity of matter flowing from underdense voids to overdense clusters is compatible with the observations in the 'real world'. If not, we should question the reliability of our simulation and check if we neglect important forces influencing the direction of the velocity flow. Figure 32 shows a slice of the Laniakea supercluster in the supergalactic equatorial plane (Tully et al. 2014).

6.3.4 Sachs-Wolfe Effect

We could also look more into the gravitational field. It can provide insight into the effect of the potential on the energy of photons passing through it - the Sachs-Wolfe effect. As photons enter the potential and climb out of it, they lose energy. This causes the photons to be redshifted each time

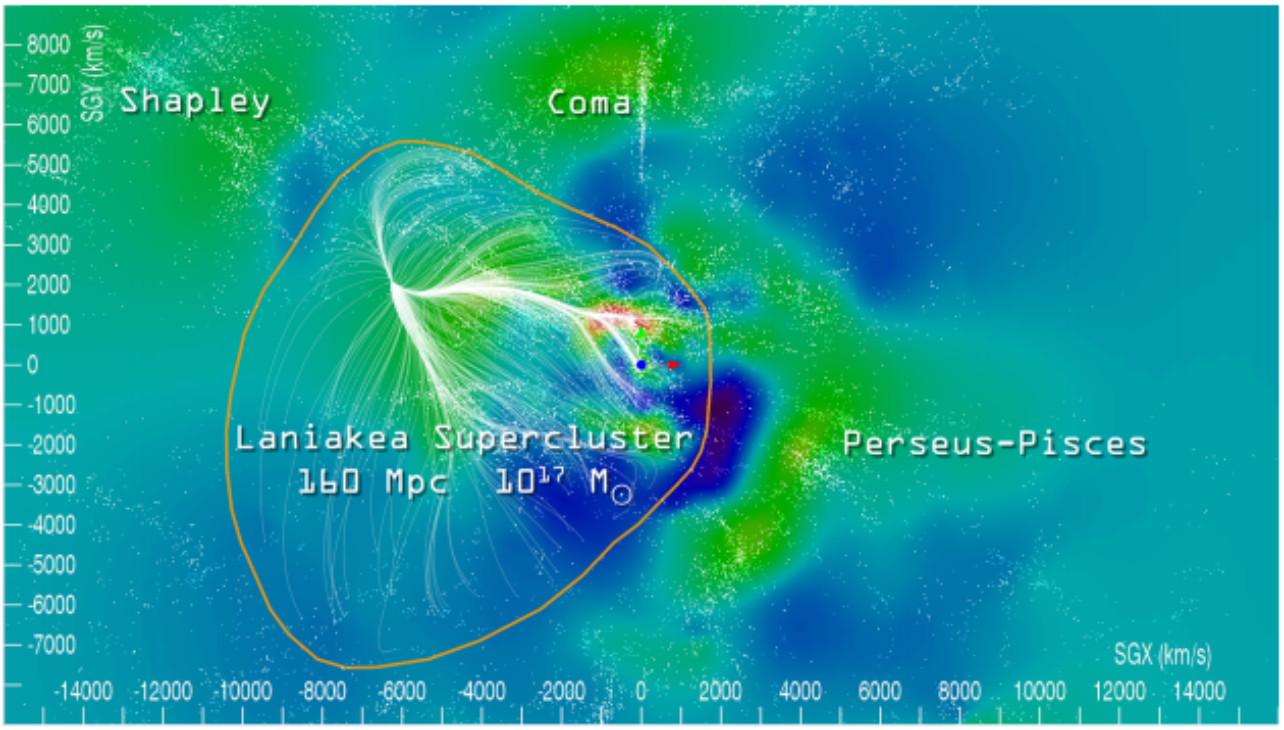

Figure 32: The Laniakea supercluster and its neighbouring clusters in the supergalactic equatorial plane. The shaded contours represent the density. Dark blue regions correspond to voids while red represents high density regions. Galaxies from a redshift catalogue are superimposed on the image as white dots. The Laniakea supercluster forms a basin of attraction, causing streams of matter (indicated as white lines) to flow its way from the low-density voids. A domain of approximately 160 Mpc in diameter is enclosing the beginning and end of the streams (indicated by the orange contour). It surrounds a mass of roughly $10^{17} M_{\odot}$ (Tully et al. 2014).

they pass a strong potential field. We can relate the shift in the potential to the CMB temperature fluctuations:

$$\frac{dT}{T} = \frac{1}{3}\frac{d\phi}{c^2}$$

For a flat Einstein-de Sitter universe where spacetime is not curved, the potential ϕ remains constant in time. By integrating over the path of the photon from the epoch of recombination we can map the potential perturbations to the total observed temperature fluctuations in the CMB:

$$\frac{\Delta T}{T} = \frac{1}{3}\frac{\phi_o - \phi_e}{c^2}$$

Where ϕ_o is the potential perturbation locally and ϕ_e is the potential perturbation at the time of last scattering. It would be better to take into account all the potential fluctuations along the path integral of the photon and not just the start and end points, because the potential is not homogeneous throughout the universe (van de Weygaert 2005). The fully integrated temperature shift along the photon's path is known as the integrated Sachs- Wolfe effect. Measuring the gravitational potential field of various simulations with different cosmological models could provide more insight into the integrated Sachs- Wolfe effect and its relation to the temperature fluctuations in the CMB and subsequently contribute evidence for a preferred cosmological model.

It would be interesting to see the gravitational potential of the DTFE density at various redshifts. We would be able to combine these snapshots to find the evolution of the potential field throughout the history of the universe. With the relation between the temperature fluctuations in the CMB and the gravitational field strength through the Sachs- Wolfe effect, we would be able to see how the potential changes the photon energy at each redshift. On the 256^3 grid of the potential field, we could transform each cell to the corresponding loss of photon energy. By comparing their PDF's at various redshifts, we could interpolate to find a trend in the derivative of the photon energy. Repeating this procedure for the different cosmological models could outline the history of the CMB photon energies and might show which model describes the anisotropies in the CMB more accurately. If the potential fields of these models are not able to describe the temperature fluctuations, we might conclude that either the Sachs- Wolfe effect isn't the only mechanism that affects the photon energy or that the determined gravitational potential isn't right. The second option would imply an incomplete theory of gravity, due to possible negligence of the repulsive effect of dark energy on the force field, and might provide useful information to construct a more thorough description.

Bibliography

Bennett, C., Larson, D., Weiland, J., Jarosik, N., Hinshaw, G., Odegard, N., Smith, K., Hill, R., Gold, B. & Halpern, M. (2013), 'Nine-year wilkinson microwave anisotropy probe (wmap) observations: final maps and results', *The Astrophysical Journal Suplement Series* **208**(20).

Blanton, M. & SDSS (2014), 'The SDSS's map of the universe', *Astronomical Journal* . arXiv:1703.00052.

Bothun, G. & McGaugh, S. (1992), 'Structural Characteristics and Stellar Composition of Low Surface Brightness Disk Galaxies', *Astronomical Journal* pp. 1–16.

Cautun, M., van de Weygaert, R., Jones, B. & Frenk, C. (2014), 'Evolution of the cosmic web', *MNRAS* pp. 2934–2938. arXiv:1401.7866.

Colberg, J., Frazer, P., Foster, C. & Platen, E. (2008), 'The Aspen–Amsterdam Void Finder Comparison Project', *MNRAS* pp. 1–14. arXiv:0803.0918.

Dries, M. (2008), 'Master Thesis: A hierarchy of voids', pp. 1–14.

Edelsbrunner, H. & Harer, J. (2001), 'Hierarchical Morse-Smale Complexes for Piecewise Linear 2-Manifolds', *Springer* pp. 2–8.

Edelsbrunner, H. & Mücke, E. (1994), 'Three-Dimensional Alpha Shapes', *ACM Transactions on Graphics* **13**(43-72), 46–51. arXiv:math/9410208v1.

Hidding, J., van de Weygaert, R. & Shandarin, S. (2016), 'The Zeldovich & Adhesion approximations and applications to the local universe', *Proceedings IAU Symposium* (308), 6.

Milnor, J. (1963), 'Morse Theory', *Princeton University Press* .

Pranav, P., Edelsbrunner, H., van de Weygaert, R., Vegter, G., Kerber, M., Jones, B. & Wintraecken, M. (2017), 'The Topology of the Cosmic Web in Terms of Persistent Betti Numbers', *MNRAS* pp. 1–7. arXiv:1608.04519v3.

Sousbie, T. (2010), 'The persistent cosmic web and its filamentary structure I: Theory and implementation', *MNRAS* pp. 4–31. arXiv:1009.4015.

Springel, V. & Max-Planck-Institute (2005), 'Millenium simulation snapshot'.

Tully, B., Shaya, E., Karachentsev, I., Courtois, H., Kocevski, D., Rizzi, L. & Peel, A. (2008), 'Our Peculiar Motion Away from the Local Void', *Astrophysical Journal* pp. 1–20. arXiv:0705.4139v2.

Tully, R., Courtois, H., Hoffman, Y. & Pomarède, D. (2014), 'The Laniakea supercluster of galaxies', *Nature* **513**(7516), 7.

van de Weygaert, R. (2005), 'Lecture Notes Linear Perturbation Theory'.

van de Weygaert, R. (2016), 'Voids and the Cosmic Web: cosmic depression & spatial complexity', *MNRAS* pp. 1–10. arXiv:1611.01222v2.

van de Weygaert, R., Bos, P., Dolag, K. & Pettorino, V. (2012), 'The darkness that shaped the void: dark energy and cosmic voids', *MNRAS* pp. 9–11. arXiv:1205.4238v2.

van de Weygaert, R., Jones, B. & Platen, E. (2007), 'A Cosmic Watershed: the WVF Void Detection Technique', *MNRAS* pp. 1–4. arXiv:0706.2788.

van de Weygaert, R., Jones, B., Vegter, G., Edelsbrunner, H., Pranav, P., Park, C., Hellwing, W., Eldering, B., Kruithof, N., Bos, P., Hidding, J., Feldbrugge, J., ten Have, E., van Engelen, M., Caroli, M. & Teillaud, M. (2013), 'Alpha, Betti and the Megaparsec Universe: on the Topology of the Cosmic Web', *Springer* pp. 14–19. arXiv:1306.3640v1.

van de Weygaert, R. & Platen, E. (2009), 'Cosmic voids: structure, dynamics and galaxies', *Modern Physics Letters A* pp. 44–57. arXiv:0912.2997.

van de Weygaert, R. & Sheth, R. (2003), 'A hierarchy of voids: Much ado about nothing', *MNRAS* pp. 1–13. arXiv:astro-ph/0311260.

Vegter, G. (2011), 'Lecture notes on Applied Geometry'.

Wilding, G. (2018), 'PhD Essay: Topological Analysis Methods for Big Data', pp. 1–21.

Wilding, G., Nevenzeel, K., van de Weygaert, R., Vegter, G., Pranav, P., Jones, B., Efstathiou, K. & Feldbrugge, J. (2021), 'Persistent homology of the cosmic web I: Hierarchical topology in ΛCDM cosmologies', *MNRAS* pp. 10–20. arXiv:2011.12851v2.

Zel'Dovich (1970), 'Gravitational instability: An approximate theory for large density perturbations', *Astronomy and astrophysics* **5**(84-89).